



## RESEARCH ARTICLE

10.1029/2018JA025355

## Ultralow Frequency Waves as an Intermediary for Solar Wind Energy Input Into the Radiation Belts

## Key Points:

- We separate the global ULF Pc5 wave activity during geomagnetic storms that produce increases and decreases in outer belt electron fluxes
- ULF waves penetrate to low  $L$  for both enhancements and depletions but persist for a prolonged period for outer belt enhancement events.
- Wave penetration depth ( $L < 2$ ) correlates with storm intensity, similarly to the penetration of the outer electron belt within the slot region

## Supporting Information:

- Supporting Information S1

## Correspondence to:

M. Georgiou,  
marina.georgiou@ucl.ac.uk

## Citation:

Georgiou, M., Daglis, I. A., Rae, I. J., Zesta, E., Sibeck, D. G., Mann, I. R., et al. (2018). Ultra-low frequency waves as an intermediary for solar wind energy input into the radiation belts. *Journal of Geophysical Research: Space Physics*, 123, 10,090–10,108. <https://doi.org/10.1029/2018JA025355>

Received 13 FEB 2018

Accepted 13 NOV 2018

Accepted article online 16 NOV 2018

Published online 13 DEC 2018

M. Georgiou<sup>1,2</sup> , I. A. Daglis<sup>2</sup> , I. J. Rae<sup>1</sup> , E. Zesta<sup>3</sup> , D. G. Sibeck<sup>3</sup> , I. R. Mann<sup>4</sup> , G. Balasis<sup>5</sup> , and K. Tsinganos<sup>2</sup>

<sup>1</sup>Mullard Space Science Laboratory, Department of Space and Climate Physics, University College London, Dorking, UK, <sup>2</sup>Department of Physics, National and Kapodistrian University of Athens, Panepistimioupolis Zografos, Athens, Greece, <sup>3</sup>Goddard Space Flight Center, National Aeronautics and Space Administration, Greenbelt, MD, USA, <sup>4</sup>Department of Physics, University of Alberta, Edmonton, Alberta, Canada, <sup>5</sup>Institute of Astronomy, Astrophysics, Space Applications and Remote Sensing, National Observatory of Athens, Penteli, Greece

**Abstract** Enhancements of electron fluxes in the outer radiation belt have been closely linked to increases in solar wind speed and density as well as to prolonged intervals of southward interplanetary magnetic field. Periodic oscillations in the Earth's magnetic field with frequencies in the range of a few millihertz (ultralow frequency or ultralow frequency waves) may be an intermediary through which these solar wind drivers influence radiation belt dynamics due to their potential for resonant interactions with energetic electrons causing the radial migration of resonant electrons. Using data from more than 180 ground magnetometers contributing to the worldwide SuperMAG collaboration, we explore possible relationships between relativistic electron flux variations and the spatial and temporal profiles of ultralow frequency wave power contained in the Pc5 frequency band (2–7 mHz). During 19 geomagnetic storms marked by relativistic ( $1.5 \text{ MeV} < E < 6 \text{ MeV}$ ) electron flux enhancements and 19 storms that led to prolonged electron flux depletions, Pc5 wave power is found penetrating to  $L$  shells as low as 2–3. The enhancement of Pc5 wave power starts almost simultaneously with the storm onset. The depth of wave activity penetration was found associated with the strength of geomagnetic activity (Spearman's  $\rho = 0.54$ ), which is also related to the location of electron flux maximum observed in the recovery phase. Pc5 wave activity persists longer (for up to  $\approx 62$  hr) for those storms that produced relativistic electrons. We also investigate the combination of interplanetary conditions necessary to differentiate the response of relativistic electron fluxes to geomagnetic storms. A coupling function that captures the increased reconnection rate at the dayside magnetopause affecting magnetospheric processes which may produce Pc5 wave power offers an additional key to further understanding the outer belt dynamics.

## 1. Introduction

Since their discovery by Van Allen et al. (1958), the Earth's radiation belts have been a subject of intense study. How this population of charged particles is accelerated to very high energies, transported and lost in the Earth's magnetosphere has been the focus of radiation belt research ever since (Kellogg, 1959). Several acceleration and loss mechanisms have been proposed to act synergistically to generate relativistic electrons whose kinetic energy can reach up to 10 MeV (Baker et al., 2014, 2016). Among the most prominent candidates are resonant interactions between electrons and extremely low frequency/very low frequency waves, which violate the first and second adiabatic invariants,  $\mu$  and  $K$  (Horne et al., 2005; Summers et al., 1998). Whistler mode chorus waves and magnetosonic waves can singly or jointly accelerate resonant electrons in situ (Li et al., 2017), and plasmaspheric hiss can cause the loss of relativistic electrons through pitch angle scattering (Ni et al., 2013).

Recent studies (Boyd et al., 2018; Chen et al., 2007) have presented compelling evidence for local acceleration as the dominant acceleration mechanism for megaelectron volt electrons in the outer radiation belt. However, radial transport by ultralow frequency (ULF) waves has also been shown to explain the outer belt dynamics (Mann et al., 2013; Su et al., 2015) and at times to be inadequate (Horne et al., 2005; Subbotin & Shprits, 2009). ULF waves with frequencies between 1 and 20 mHz (Jacobs et al., 1964) can violate the third adiabatic invariant  $L^*$  under the drift resonance condition  $\omega = m \cdot \omega_d$ , where  $\omega$  is the wave frequency,  $m$  the azimuthal wave mode

©2018. The Authors.

This is an open access article under the terms of the Creative Commons Attribution License, which permits use, distribution and reproduction in any medium, provided the original work is properly cited.

number, and  $\omega_d$  the electron drift frequency (Elkington et al., 2003; Ozeke et al., 2014).  $L^*$  is Roederer's drift shell parameter (Roederer, 1970), which is equal to the radial distance of the adiabatically equivalent electron drift orbit on the equatorial plane of a dipole field. The importance of radial transport for the outer radiation belt evolution during geomagnetic storms has not been determined definitively.

Radial transport is often described as a stochastic process, whereby a source population at large radial distance (e.g., from the plasma sheet; Turner, 2010) is transported earthward to regions of stronger geomagnetic fields and, thereby, electrons increase their energy. Inward radial diffusion is the result of incoherent transport of particles by fields fluctuating stochastically at electron drift frequencies. Radial diffusion may also act as a loss mechanism when particles drift outward and are lost to the magnetopause (Hudson et al., 2014; Loto'aniu et al., 2010; Ozeke et al., 2014). The direction of particle diffusion (inward or outward) is dependent on the gradient of electron phase space density in adiabatic coordinates,  $\mu$ ,  $K$ , and  $L^*$  (Green & Kivelson, 2004). Non-diffusive prompt transport has been identified as an additional source of relativistic electrons for the outer radiation belt (Brautigam & Albert, 2000; Fälthammar, 1965, 1968). Such rapid acceleration is typically mediated by shock-induced compressional waves (e.g., the case of 24 March 1991 superstorm; Blake et al., 1992; Li et al., 1993).

The diffusion rate is proportional to power spectral density (PSD) of stochastic fluctuations of the Earth's magnetic field as well as induced electric fields in the ULF frequency range (Fei et al., 2006). The radial diffusion coefficient ( $D_{LL}$ ) describing the diffusion rate of energetic electrons increases with  $L$  shell (Brautigam & Albert, 2000; Huang et al., 2010; Ozeke et al., 2012) since power progressively decreases toward the inner magnetosphere (Georgiou et al., 2015; Liu et al., 2009). This monotonic relationship has been evident in the correlation observed at times between solar wind speed increases and outer radiation belt electron flux enhancements (Liu et al., 2010; Mann et al., 2004; Mathie & Mann, 2000, 2001; O'Brien, Sornette, & McPherron, 2001). Increased ULF wave power should correspond to an increase in  $D_{LL}$  and, therefore, faster radial diffusion resulting in electron flux enhancements during geomagnetic storms.

In this paper, we extend the previous study reported by Georgiou et al. (2015) on the association between outer belt electron flux and ULF Pc5 wave power enhancements. By exploiting the benefits of combining magnetic field data from multiple ground magnetometer arrays into a global network by the SuperMAG initiative (Gjerloev, 2009), Georgiou et al. (2015) derived the latitudinal and azimuthal distribution of Pc5 wave power during the initial, main, and recovery phase of four intense magnetic storms (minimum  $Dst$  index ranged from  $-105$  to  $-387$  nT). The results indicated that electron flux enhancements were associated with wave power penetrating deep into the inner magnetosphere. In addition, the penetration depth was found to be proportional to the storm strength (we refer the reader to Figures 3 and 6 of Georgiou et al., 2015). It is, however, essential to go beyond case studies and look at statistics and a bigger picture to tease out the effect of Pc5 wave activity on outer radiation belt electrons, and this is the aim of our study.

The superposed epoch analysis of ULF Pc5 wave activity during 38 intense and moderate storms ( $-220$  nT  $< SYM - H_{min} < -40$  nT) that occurred during the previous solar cycle 23 allows us to look into the importance of magnetospheric versus solar wind conditions when studying the storm response of the outer belt electron fluxes. In section 2, we present the relativistic electron flux enhancement and depletion events selected to investigate which had been initiated by coronal mass ejections (CMEs), but the response of the geomagnetic field and plasma populations in the magnetosphere was different. This difference had previously been investigated by O'Brien, et al. (2001, 2003). Taking these past studies a step further, observations presented in this paper draw a comprehensive picture of the distribution of ULF Pc5 wave activity along radiation belt electron drift paths and  $L$  shells. In section 3, solar wind and solar wind-magnetosphere coupling parameters are first investigated for the two sets of geomagnetic storms with and without relativistic electron flux enhancements in the recovery phase. Within the magnetosphere, changes in the relativistic electron population of the outer radiation belt are, subsequently, compared against ULF Pc5 wave activity that also varied in both intensity and duration between storms that produced or did not produce relativistic electrons. In section 4, we discuss our results which are summarized in section 5.

## 2. Data Set and Analysis

### 2.1. Event Selection

We focus on isolated geomagnetic storms that occurred between January 1998 and April 2004, a period covering most of the ascending phase of solar cycle 23, through the maximum, to the early declining phase.

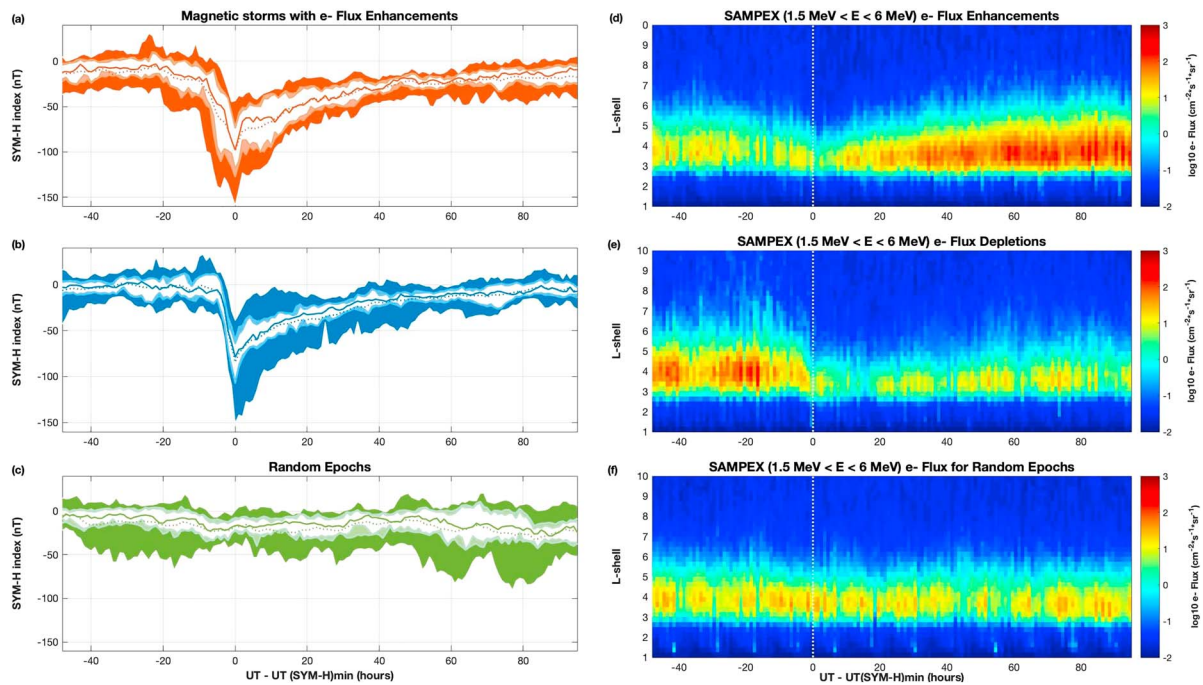


**Figure 1.** Superposed epoch analysis of *SYM-H* index and relativistic electron fluxes measured by the SAMPEX satellite for magnetic storms leading to flux enhancements in the recovery phase (a, d), sustained flux depletions (b, e), and a set of random epochs (c, f). The dotted vertical line denotes the time of *SYM-H* index minimum, which we define as epoch time zero,  $t_0$ . SAMPEX = Solar Anomalous and Magnetospheric Particle Explorer; UT = Universal Time.

To avoid the influence of multiple storms, we limited our study to isolated storms with no other storms occurring within 2 days before and at least 3 days after, whose origin was traced back to either an interplanetary coronal mass ejection (ICME) or a magnetic cloud (Gopalswamy et al., 2009; Lepping et al., 2006; Richardson & Cane, 2010; Zhang et al., 2007). A total of 38 intense (with  $SYM - H_{\min} < -100$  nT) and moderate storms (with  $SYM - H_{\min} < -40$  nT) with one-step growth in *SYM-H* index followed by a recovery to prestorm levels without additional activity was found to satisfy these criteria. The number of selected storms with the classic profile is a fraction of the storms that had been accounted in the previous study of O'Brien, et al. (2001, 2003) which, in their vast majority, had developed in a more complicated fashion. Using this list of storms (Tables S1 and S2 of supporting information), we performed superposed epoch analyses on relativistic electron flux measurements as well as solar wind parameters, ULF Pc5 wave power, and Pc5 wave activity index. We followed the methodology of Morley and Freeman (2007), Morley et al. (2010), and Hendry et al. (2005) for superposed epoch analysis with the minimum of *SYM-H* index, marking the maximum of each magnetospheric disturbance as epoch time zero,  $t_0$ , and separated storms into storms that result in electron flux enhancement or prologued depletion.

Figures 1a–1c show the superposed epoch median of *SYM-H* index by a solid line and mean with a dotted line. The 95% confidence interval for the median, shown by the white-colored band, is the bias-corrected and accelerated bootstrap interval. The light-colored bands indicate the interquartile range and the dark-colored line the bootstrapped 95% confidence interval about it. To obtain the confidence intervals for the median, 1,000 bootstrap samples were used and 4,000 for the confidence intervals about the interquartile range. The superposed epoch of *SYM-H* index gives confidence in our method of single-dip storm identification since it shows the expected morphology of storm evolution. However, stronger storms have been known to behave differently from weaker storms in that the timescales of both main and recovery phases are longer (Yokoyama & Kamide, 1997). For each of the two sets of storms, the durations of the main and, in particular, the initial recovery phase have quite a large range, generating the large spread of the index values. The *SYM-H* index falls off somewhat quicker in the events that did not produce high-energy electrons in the recovery phase, suggesting that the geomagnetic field topology was likely different than events that result in relativistic electron flux enhancements.

## 2.2. Relativistic ( $E \geq 1.5$ MeV) Electron Flux Measurements

To examine enhancements and depletions in the outer belt electron fluxes, we used measurements of relativistic electron fluxes from National Oceanic and Atmospheric Administration's Geostationary Operational Environmental Satellites (GOES). The energetic particle sensor EP8 onboard GOES-8 and GOES-10 measured the integral directional flux of electrons at energies  $\geq 2$  MeV (Onsager et al., 1996). The relativistic electron flux measurements were extrapolated to local noon in order to distinguish temporal variations from the consequences of the orbital motion of satellites using Statistical Asynchronous Regression, as proposed by O'Brien, Sornette, & McPherron (2001) to determine the relationship between two quantities without simultaneous measurements. In addition, measurements of integral directional electron fluxes at 1.5–6 MeV from the Proton/Electron Telescope instrument onboard the Solar Anomalous and Magnetospheric Particle Explorer (SAMPEX; Cook et al., 1996) were used as representative of conditions in the radiation belts. The near-polar orbit of SAMPEX at an altitude of  $\approx 600$  km and a period of  $\approx 96$  min allowed the collection of observations of both trapped and precipitating relativistic electrons in the outer radiation belt (Tu et al., 2010). The measurements recorded have been averaged and sorted by the McIlwain  $L$  shell to produce the radial profile of relativistic electron fluxes for  $L$  shells ranging from 1 to 10 with spatial resolution up to  $0.25 L$  (we refer the reader to Figure S1).

To determine each storm's response, we used the criterion applied by Reeves et al. (2003) on relativistic electron fluxes measured by the GOES satellites. The maximum electron flux measured by GOES satellites over a period of time of 2 days prior to the  $SYM-H$  minimum was compared with that 4 days after. When the ratio of the prestorm to poststorm maximum electron flux was found to be greater (or lower) than a factor of 2, the electron flux change at geosynchronous orbit was defined as an enhancement (or depletion) and this was in agreement with the electron flux change observed at different  $L$  shells by the SAMPEX spacecraft. Figures 1d–1f show the results of superposed epoch analysis where relativistic electron fluxes measured by SAMPEX have been binned according to epoch time (1-hr resolution) and  $L$  shell ( $0.25-L$  resolution) from 2 days prior to the disturbance maximum to 4 days following  $t_0$  based on Universal Time (UT). In addition to the two sets of storms marked by electron flux enhancements and prolonged depletions, superposed epoch analysis was undertaken with a set of 20 random epochs within the period 1998–2004 as a check of the significance of changes observed during geomagnetic storms.

Specifically, Figure 1d shows the median of 1.5- to 6-MeV electron fluxes observed during 19 magnetic storms that led to flux enhancements in their recovery phase.  $t_0$  marked by the dotted line corresponds to the minimum  $SYM-H$  index during each magnetic storm. Prior to the  $SYM-H$  index minimum, relativistic electron fluxes reached values as high as  $10^3 \text{ cm}^{-2} \cdot \text{s}^{-1} \cdot \text{sr}^{-1}$  and spread over a region extending from  $\approx 2.5$  to  $\approx 5.9 L$  (with this  $L$  shell range defined by flux  $> 10^1 \text{ cm}^{-2} \cdot \text{s}^{-1} \cdot \text{sr}^{-1}$ ). Relativistic electron fluxes fell during the storms' main phase, gradually recovered, and eventually surpassed prestorm levels in the recovery phase. It is worth noting the difference between the electron fluxes observed in the recovery phase of 19 storms leading to enhancements and storms followed by sustained flux depletions (Figure 1e). In particular, relatively low values and a maximum of  $\approx 28 \text{ cm}^{-2} \cdot \text{s}^{-1} \cdot \text{sr}^{-1}$  were observed during the recovery phase of storms followed by flux depletions that did not exceed  $\approx 316 \text{ cm}^{-2} \cdot \text{s}^{-1} \cdot \text{sr}^{-1}$ . While only the median of the electron fluxes from SAMPEX are shown here, the changes are consistent with the lower and upper quartiles as well as the mean of the flux distribution (not shown here).

## 2.3. ULF Pc5 Wave Power Observations

To determine how ULF Pc5 wave activity evolved during the selected storms, we exploited magnetic field data made available by the SuperMAG initiative that brings together magnetic field measurements from more than 30 ground magnetometer arrays. For consistency between the magnetic coordinates provided for Proton/Electron Telescope electron measurements in SAMPEX mission data archives, the International Geomagnetic Reference Field (IGRF) 1990 model has also been used for the calculation of ground magnetometer magnetic coordinates and in particular,  $L$  shell. To calculate ULF wave power in the Pc5 frequency range, we adopted the methodology of Balasis et al. (2012) and Balasis et al. (2013) for the continuous wavelet transform analysis of the magnetic north horizontal (N) component in the measured geomagnetic field. From the dynamic wavelet spectra, we calculated the scale-averaged wavelet power over the frequency range between 2 and 7 mHz (corresponding to periods of 150 to 600 s). We also calculated the scale-averaged wave power at all frequencies above 0.2 mHz and up to the Nyquist frequency (equal to 8.3 mHz for 1-min resolution data available through SuperMAG) to derive a Pc5 ULF wave activity index. These calculations were performed

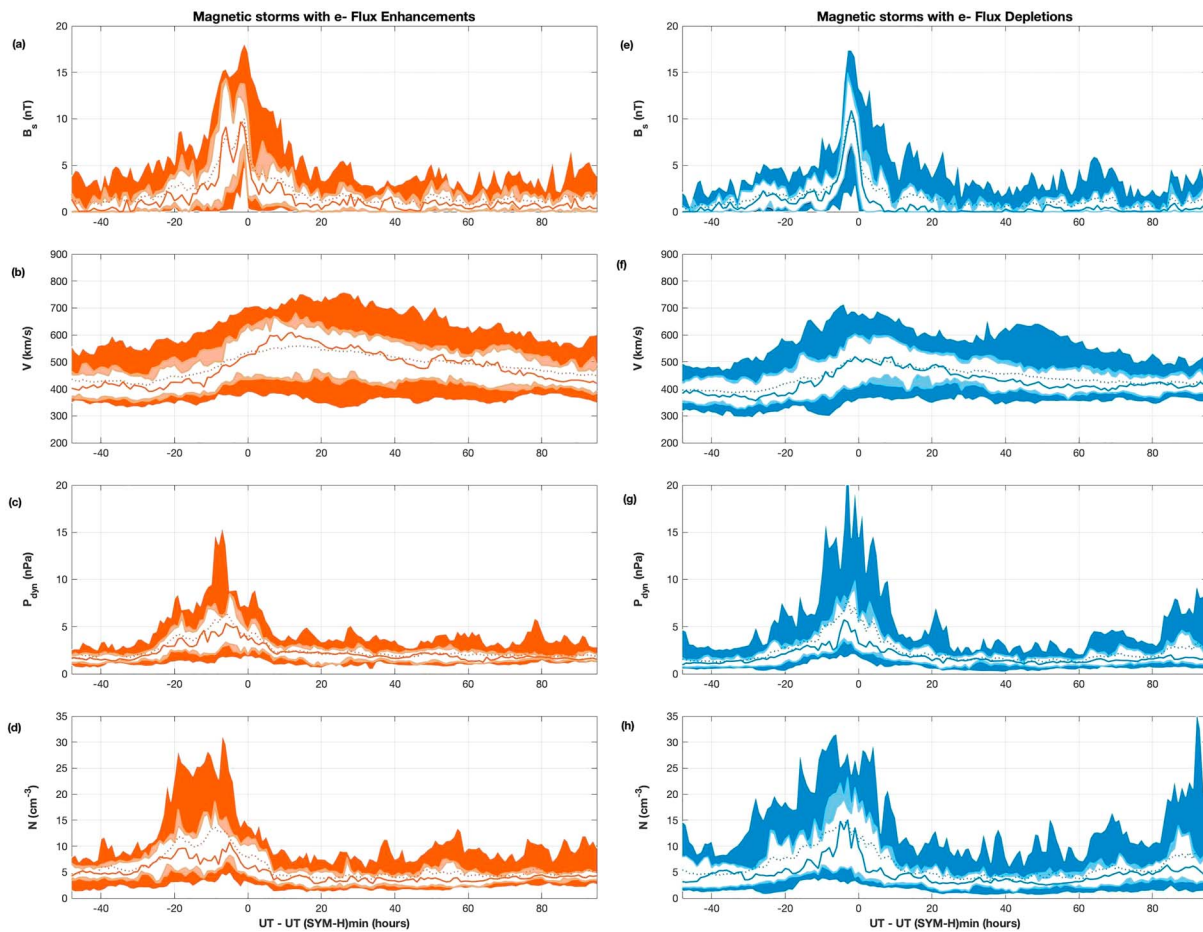


**Figure 2.** (a–h) Superposed epoch analysis of half-wave rectified interplanetary magnetic field  $B_z$ , solar wind speed, dynamic pressure, and proton density, as measured by the ACE/Wind spacecraft for the same two storm sets as Figure 1. UT = Universal Time.

in order to be able to differentiate between power concentrated in the Pc5 frequency range in the form of narrowband pulsations from more broadband power.

Specifically, we followed the approach of Engebretson et al. (1998) and Posch et al. (2003) who had defined such a Pc5 wave activity index as the ratio of power integrated over the Pc5 frequency band to the power integrated over the wider  $\geq 0.2$ -mHz frequency band to identify the dominance of narrowband Pc5 pulsations. Since spectral power falls as  $f^{-2}$ , this index is primarily sensitive to the ratio of wavelet power above 2 mHz to power in the 0.2–2 mHz. Therefore, increasing values of the index indicate that more wavelet power is concentrated in the Pc5 frequency band in the form of narrowband pulsations rather than in broadband noise, which may have been generated by substorm activity or irregular pulsations. A different approach had been followed by Kozyreva et al. (2007) to calculate a similar ULF wave activity index and reached similar results as Engebretson et al. (1998) and O'Brien, Sornette, and McPherron (2001; we refer the reader to Figure 3 of Kozyreva et al., 2007).

### 3. Superposed Epoch Analysis Results

#### 3.1. IMF and Solar Wind Conditions

Figure 2 shows the results of superposed epoch analysis for a set of parameters in the solar wind that we analyzed for the selected storms. Similar to Figure 1,  $t_0$  has been defined as the UT of minimum *SYM-H* index. In addition to the median and the 95% confidence interval for the median, each panel also shows the interquartile range and 95% confidence interval about it for the half-wave rectified interplanetary magnetic field (IMF)  $B_z$  component in Geocentric Solar Magnetospheric coordinates,  $B_s$ , the solar wind flow speed,  $V_{sw}$ , proton density,  $N$ , and dynamic pressure,  $P_{dyn}$ , at every hour of epoch time.

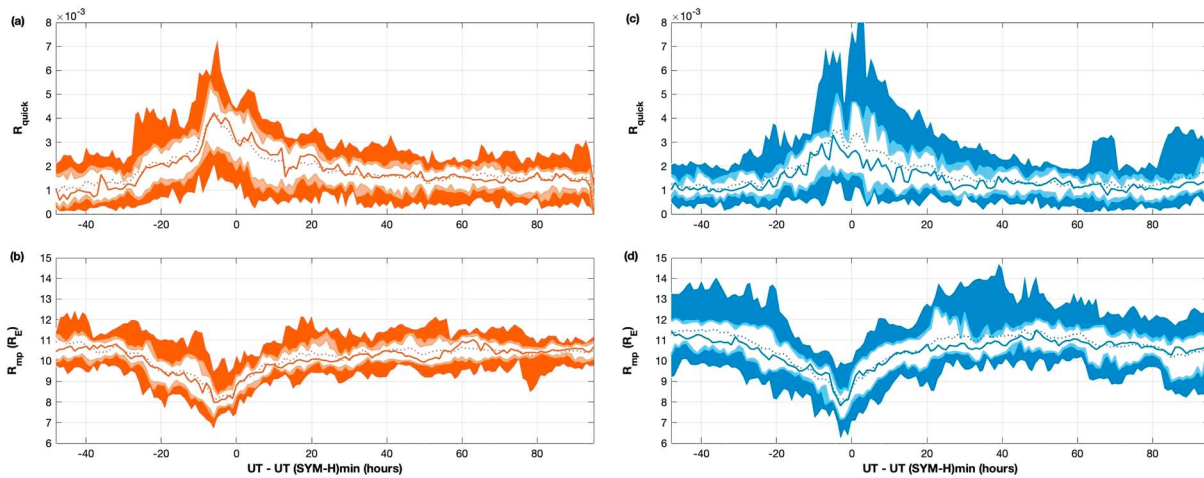


**Figure 3.** Superposed epoch analysis of magnetic reconnection rate at the dayside magnetopause (a, c) and magnetopause location (b, d) in the same format as Figure 2. UT = Universal Time.

$B_s$  shown in Figures 2a and 2e, where  $B_s = -B_z$  when  $B_z \leq 0$  and  $B_s = 0$  when  $B_z > 0$ .  $B_s$  offers a measure of the efficiency of magnetic reconnection at the dayside magnetopause that is favored by southward IMF orientation (Dungey, 1961). Southward IMF  $B_z$  also influences the megaelectron volt electron population in the outer radiation belt (Wing et al., 2017; Zhao et al., 2017). Specifically, southward IMF  $B_z$  has been proposed as a requirement for relativistic electron enhancements (Iles et al., 2002). This is evident in storms leading to flux enhancements where the  $B_s$  remained at high levels longer during both the main phase and early recovery (up to  $t_o + 20$  hr) than storms followed by prolonged depletions. *Shut off* of the  $B_s$  influence is observed earlier in storms followed by prolonged depletions without continued energy input into the magnetosphere.

When considering the solar wind flow speed, we see that  $V_{sw}$  drops off gradually during the recovery phase of storms that did not produce relativistic electrons but remains at high levels ( $>500$  km/s at  $t_o + 62$  hr) in events that produced (Figure 2b and 2f). The median  $V_{sw}$  (close to 500 km/s at  $t_o - 2$  hr) peaks during the main phase of storms with prolonged flux depletions and in the early recovery phase ( $\approx 600$  km/s at  $\approx t_o + 6$  hr) of storms where relativistic electrons responded above prestorm levels. Previous studies have suggested that  $V_{sw}$  is a dominant driver of relativistic electron fluxes in the outer radiation belt (Kellerman & Shprits, 2012; Paulikas & Blake, 1979; Reeves et al., 2011, 2013). Moreover, Lyatsky and Khazanov (2008) found that the response of relativistic electrons along the geosynchronous orbit to an increase in the solar wind speed has a lag time of  $\approx 2$  days. Our results support a similar conclusion to these as well as other studies.

In contrast with the southward IMF and solar wind speed, the solar wind dynamic pressure  $P_{dyn}$  (Figures 2c and 2g) remains for most storms leading to electron flux enhancements at lower values ( $< 8$  nPa) even though the same fluctuations on average are seen as during storms followed by flux depletions. Li et al. (2005) have suggested that  $P_{dyn}$  increases push the magnetopause inward. This compression of the magnetopause, which presumably opens up to previously closed particle drift paths, leads to trapped electrons crossing the magnetosphere's outer boundary and being lost into the interplanetary medium—a physical process known as magnetopause shadowing of drift paths (Katsavrias et al., 2015; Kim et al., 2008; Shprits et al., 2006; Ukhorskiy et al., 2015). Yu et al. (2013) estimated that magnetopause shadowing accounts for more than 90% of the flux dropout observed at geosynchronous orbit during the main phase of storms and  $\approx 60\%$  at lower  $L$  shells. The increase in  $P_{dyn}$  is contained in the initial and main phases of storms (between  $t_o - 24$  hr and  $t_o + 12$  hr) after which the solar wind dynamic pressure recovered, resulting in relaxation of the magnetopause that is discussed in section 3.2.

Solar wind density,  $N$ , shown in Figures 2d and 2h, has been associated with enhancements of plasma sheet density (Borovsky et al., 1998). In addition, increased solar wind density can reduce penetration of large-scale electric fields into the inner magnetosphere, increasing the size of the plasmasphere and plasmaspheric plumes (Onsager et al., 2012). Our selection of storms seems to have resulted in a set of events with different density profile in the solar wind where higher density median is observed in events followed by electron flux depletions (up to  $\approx 14$   $\text{cm}^{-3}$ ) than during events leading to flux enhancements ( $\approx 9$   $\text{cm}^{-3}$ ). These results do

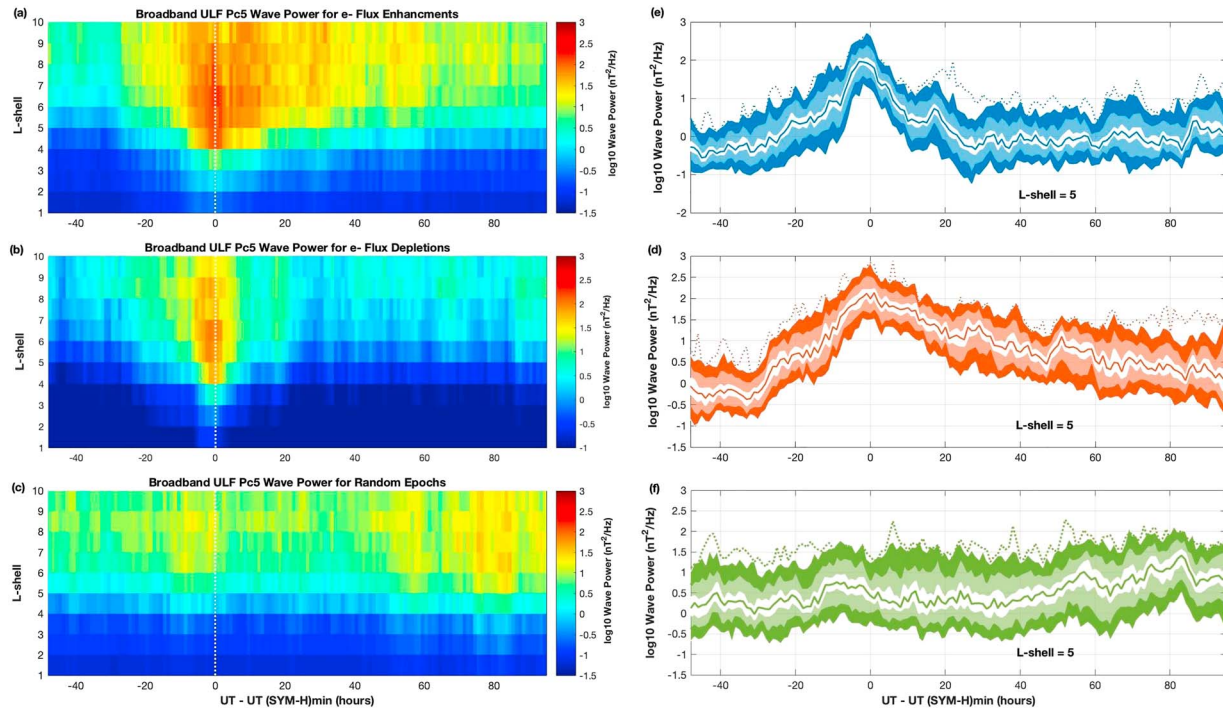


**Figure 4.** Superposed epoch analysis of broadband Pc5 wave power in the north horizontal component as measured by ground magnetometer arrays collaborating with SuperMAG for storms leading to flux enhancements (a, d), sustained flux depletions (b, e), and a set of random epochs (c, f). The superposed median (white line) and mean (dotted black line) of power at  $L=5$  are shown on the right along with the interquartile range and 95% confidence interval about them. ULF = ultralow frequency; UT = Universal Time.

not show conclusively that solar wind proton density shows the opposite behavior to outer belt electron flux but are consistent with Lyatsky and Khazanov (2008) and Kellerman and Shprits (2012).

### 3.2. Solar Wind-Magnetosphere Coupling

Besides solar wind and IMF parameters, a number of solar wind-magnetosphere coupling functions have been proposed over the years to quantify the effect of solar wind on geomagnetic activity. The *epsilon* parameter of Akasofu,  $\epsilon = (4\pi/\mu_0)V_{sw}B^2\sin^4(\theta/2)l_o^2$ , where  $\mu_0$  is the magnetic permeability of free space and  $l_o$  is an empirically determined scaling factor corresponding to the estimated energy input in the magnetosphere (Akasofu, 1991), is widely used although its unclear definition may lead to confusing interpretations. The reconnection rate at dayside magnetopause derived according to the Cassak-Shay equation (Borovsky & Birn, 2014), shown in Figures 3a and 3c, is closely correlated with geomagnetic activity indices. When looking at the median of  $R_{quick}$ , the peak at  $\approx t_o - 8$  hr was reached within the main phase of both sets of storms. Nonetheless, on average,  $R_{quick}$  remained at higher levels in the main phase as well as the early recovery phase (up to  $t_o + 36$  hr) of those storms that produced relativistic electrons.

Magnetic reconnection occurs at the magnetopause where energy, mass, and momentum are transferred from the magnetosheath into the magnetosphere. In investigating interactions between the interplanetary and near-Earth space environment, determination of the size and configuration of the magnetosphere are, therefore, also important. We used the Shue et al. (2006) model to calculate the magnetopause location. As shown in Figures 3b and 3d, during storms that produced sustained losses of high-energy electrons, there was substantial dayside compression of the magnetopause ( $R_{mp} < 8 R_E$  at about  $t_o - 4$  hr). While the innermost location reached was on average similar between the two sets of storms, the magnetopause had moved inward of  $7 R_E$  during the most intense storms leading to sustained electron flux depletions. The difference in  $R_{mp}$  as well as  $R_{quick}$ ,  $N$ ,  $P_{dyn}$ ,  $V_{sw}$ , and  $B_s$  between the two sets of storms with different response of outer belt electron fluxes was confirmed by Kolmogorov-Smirnov testing carried out at a statistical significance level of 5% and over the time period from  $t_o - 26,05$  hr to  $t_o + 66,82$  hr, which corresponds to the average duration of storms examined.

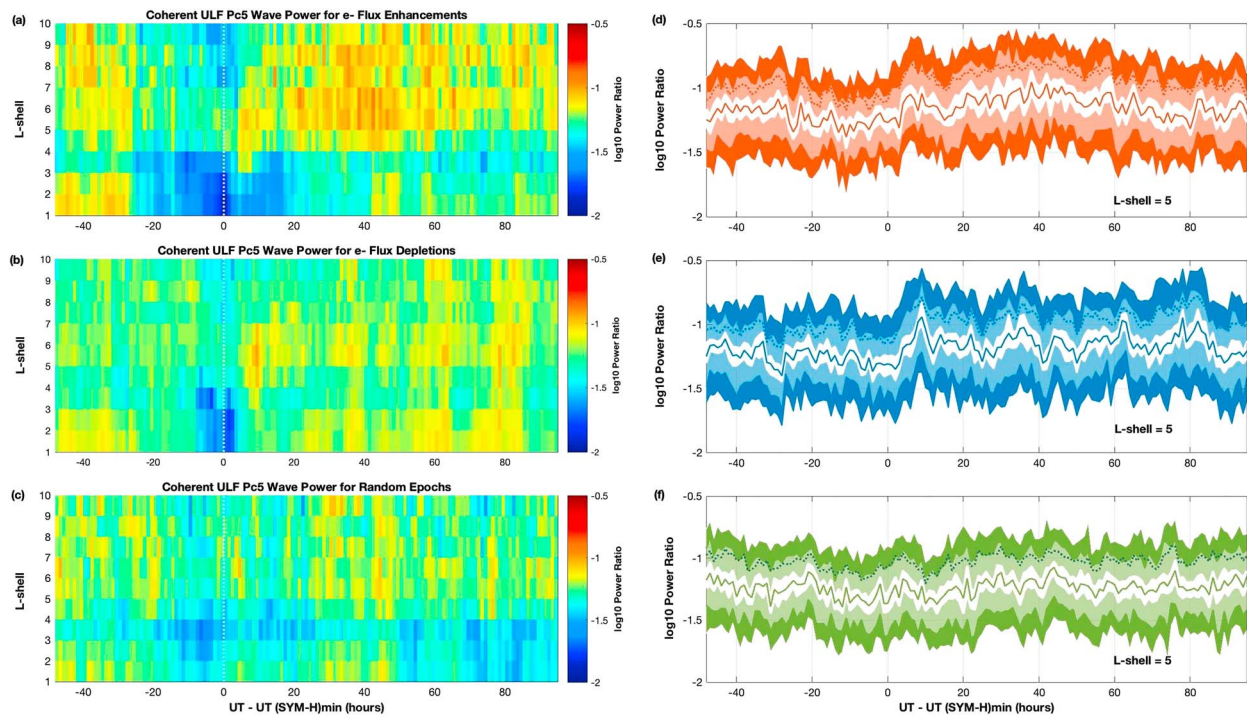


**Figure 5.** Superposed epoch analysis of coherent narrowband Pc5 wave power in the north horizontal component as measured by ground magnetometer arrays collaborating with SuperMAG for storms leading to flux enhancements (a, d), sustained flux depletions (b, e), and a set of random epochs (c, f) in the same format as Figure 4. ULF = ultralow frequency; UT = Universal Time.

While the solar wind structure for the storms investigated was similar in that either an ICME or a magnetic cloud, which is a subset of ICMEs (Richardson & Cane, 2004), was the origin, differences between these interplanetary structures could be responsible for the broad range of the superposed epoch of solar wind parameters. Specifically, 30% of the storms were associated with magnetic clouds and more than half (57.5%) with sheath fields/plasma regions formed ahead of the ICME ejecta. Echer et al. (2008) have shown that both intense and moderate storms may be caused by equally high solar wind dynamic pressure (shocks), high speed streams, and IMF  $B_z$  north conditions. However, magnetic cloud and sheath driving had a different response from the Earth's magnetosphere than CMEs. Sheaths, ejecta, and magnetic clouds are characterized by distinct solar wind and IMF conditions as well as different magnetospheric responses, and it is, therefore, expected that they also have distinct effects on the radiation belt dynamics (Hietala et al., 2015). For example, the depleting effect of sheath regions is clearly seen in the 23 May 2002 storm driven by a sheath alone.

### 3.3. ULF Pc5 Wave Power Spatiotemporal Distribution

#### 3.3.1. Latitudinal Pc5 Wave Power Distribution

Figure 4 shows the median of Pc5 wave power concentrated in the magnetic north horizontal component ( $N$ ) of the geomagnetic field as a function of epoch time relative to minimum  $SYM-H$  index over  $L$  shells ranging from 1 to 10. In both sets of storms that have produced relativistic electrons in the recovery phase and storms that resulted in sustained electron depletions, Pc5 wave power decreased with decreasing  $L$  shell while its peak is observed almost simultaneously with the minimum  $SYM-H$  index. As shown in Figures 4a and 4d, Pc5 wave power reached its highest values (higher than  $10^2$  nT<sup>2</sup>/Hz) during the main phase and was sustained throughout the recovery (up to  $\approx t_o + 48$  hr) of those magnetospheric events that led to electron flux enhancements. We should also note that Pc5 wave activity was not only limited in the recovery phase of storms followed by prolonged flux dropouts (Figures 4b and 4e); it also dropped off by more than an order of magnitude  $\approx 8$  hr after the  $SYM-H$  index minimum. This striking difference is consistent with the previous studies of O'Brien, Sornette, and McPherron (2001) and O'Brien et al. (2003) and points out the role that ULF Pc5 waves may play in accelerating electrons and populating the outer radiation belt with high-energy particles.

Figure 5 shows the time evolution of the median of Pc5 wave activity index at  $L$  shells ranging from 1 to 10. The specific index has been calculated as the ratio of power integrated over the Pc5 frequency band to the power within the wider  $\geq 0.2$ -mHz frequency band. Although it does not indicate the magnitude of Pc5

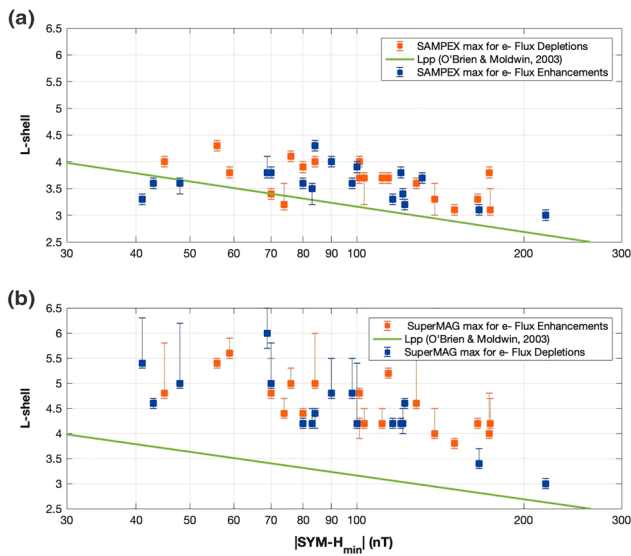


**Figure 6.**  $L$  shell of the maximum electron flux (a) and maximum Pc5 wave power (b) versus minimum  $SYM-H$  index for the same storm sets as Figures 1 and 4. Vertical bars represent where the flux and power are greater than 85% of the maximum value. The green solid line shows the scaled plasmopause model  $L_{pp}$  of O'Brien and Moldwin (2003). SAMPEX = Solar Anomalous and Magnetospheric Particle Explorer.

waves, this index is an indicator of coherent pulsations observed mainly before the onset of storms resulting in electron flux enhancements and more pronounced in the recovery phase (Figures 5a and 5d). The larger values of the index ( $>0.1$ ) correspond to intervals of enhanced Pc5 wave activity over roughly constant background, peaking at  $L$  shells between  $\approx 4$  and 9. During the recovery phase of storms followed by sustained flux depletions (Figures 5b and 5e), on the contrary, the index remained at lower values (between 0.05 and 0.1) at all  $L$  shells—either suppressed or masked by more broadband Pc5 wave activity. The peak of the index was observed at  $L$  shells between 5.5 and 6.5. These observations of coherent Pc5 wave activity observed to be related to enhancements of relativistic electron fluxes in the recovery phase of storms are consistent with coherent drift resonant acceleration of electrons to the high energies that characterize the outer radiation belt (Degeling et al., 2008; Degeling & Rankin, 2008), as well as narrowband Pc5 waves observed to resonate and modulate electron populations at geosynchronous orbit (Sarris et al., 2007).

### 3.3.2. $SYM-H$ -Dependent Penetration in the Slot Region

The broad intensity range of storms selected for this study, with minimum  $SYM-H$  index ranging from approximately  $-40$  to  $-220$  nT revealed an association between storm intensity and  $L$  shell position of the peak flux of relativistic electrons, which had been first observed by Williams et al. (1968) and has been confirmed by recent studies (i.e., Tverskaya et al., 2003; Zhao & Li, 2013). Figure 6 shows the  $L$  shell location of maximum relativistic flux (panel a) as well as of the maximum Pc5 wave power observed

during each of the 38 storms of this study (panel b). An example of the analysis methodology adopted to identify the location of each maximum is shown in Figure S1 of the supporting information. Uncertainties in the  $L$  shell position are shown as vertical bars representing where wave power and electron flux are greater than 85% of their maximum value at the peak of each storm and at the maximum of the outer radiation belt penetration in the slot region, similar to Zhao and Li (2013).

Despite these uncertainties, the  $L$  shell position of the maximum did not cross the plasmopause—except for the weaker storms examined. The outer layers of the plasmasphere are believed to be stripped off during periods of geomagnetic activity, bringing the plasmopause to  $L$  shells as low as 2. The work of O'Brien and Moldwin (2003) has shown that the location of the plasmopause can be modeled as a function of the minimum  $Dst$  index observed over the past 24 hr as follows:  $L_{pp} \approx 6.3 - 1.57 \cdot \log_{10} |\min_{[-24,0]} Dst|$  without regard to the local time dependence. Interestingly, this  $L_{pp}$  model resembles the  $L_{max}$  model developed by Tverskaya et al. (2003) for outer belt electron fluxes, and moreover, it fits the  $SYM-H$  dependence observed in the maximum Pc5 wave power.

A monotonic relationship of the level of geomagnetic activity and the Pc5 wave power peak is evident in Figure 6b for both storms leading to flux enhancements and sustained flux depletions. During the main phase of the most intense storms, enhanced Pc5 wave power was observed to peak at  $L$  shells lower than 4. During half of the storms examined, the electron flux at geosynchronous orbit increased in the recovery phase, while for the other half the flux decreased. This difference in the response of the outer radiation belt electron fluxes was independent of the specific  $L$  shell (of the geosynchronous orbit). The decrease in relativistic electron fluxes which did not recover during three of the weakest storms may explain the weak correlation between the  $L$  shell of maximum electron flux and minimum  $SYM-H$  index (Spearman's  $\rho$  of 0.46) but not between the  $L$  shell of maximum Pc5 wave power and minimum  $SYM-H$  index (Spearman's  $\rho$  of 0.54) for the 38 storms selected to be examined. Penetration of enhanced wave activity dependent on the level of geomagnetic activity seems to be expected only during storms with minimum  $SYM-H$  index  $< -50$  nT.

### 3.3.3. Local Time Pc5 Wave Power Distribution

Figure 7 illustrates the median of Pc5 wave power contained in the magnetic field's  $N$  component as a function of epoch time relative to minimum  $SYM-H$  index over all local times. Pc5 wave power in both sets of storms increases in the main phase but reaches values more than an order of magnitude higher ( $> 10^{1.5}$  nT<sup>2</sup>/Hz) in the early recovery phase of storms leading to electron flux enhancements before gradually decreasing later than

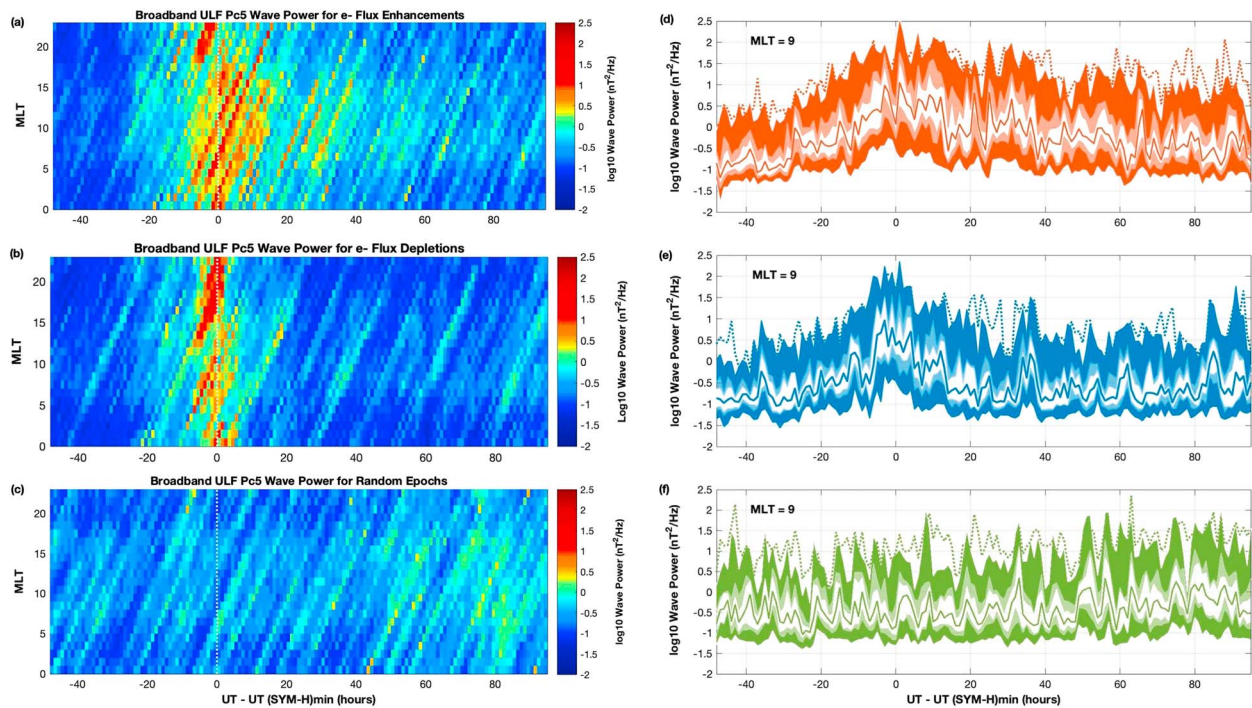


**Figure 7.** Superposed epoch analysis of broadband Pc5 wave power in the north horizontal component as a function of MLT for storms leading to electron flux enhancements (a, b), sustained electron flux depletions (b, e), and a set of random epochs (c, f) in the same format as Figure 4. ULF = ultralow frequency; MLT = magnetic local time.

$t_o + 56$  hr. We should also note that the local time distribution of Pc5 wave power peaks in the premidnight and dawn sector (from 18:00 to 24:00 UT and from 03:00 to 09:00 UT, respectively).

In situ measurements can reveal compressional, azimuthal, as well as radial components of magnetic field fluctuations, while signals detected on the ground are mostly of transverse components and Pc5 waves of low azimuthal wave number that traverse the ionosphere. Still, we see a premidnight peak where it has been observed in GOES magnetic field data analyzed by Huang et al. (2010) and is likely the consequence of storm or substorm activity driven by tail processes, including substorm injections and dampened oscillatory flow in the plasma sheet. Lyons et al. (2002) had argued that large-scale ULF waves that strongly perturb the plasma sheet are a major component of tail dynamics during periods of enhanced convection. These ULF waves occasionally have amplitudes as large as plasma flow changes that occur in association with auroral zone disturbances, such as substorms. On the other hand, the noon sector wave activity seen during storms followed by prolonged electron flux depletions (Figure 7c) was likely driven by solar wind dynamic pressure variations that perturb the dayside magnetopause at ULF wave frequencies (Kepko et al., 2002).

Figure 8 shows that, after having decreased to  $< 0.05$  during the main phase of both sets of storms, at magnetic local time (MLT) between 09:00 and 10:00, our Pc5 wave activity median remained  $> 0.11$  for most of the recovery phase of storms leading to electron flux enhancements (longer than 80 hr) and  $> 0.9$  during the recovery phase of storms resulting in sustained flux depletions. In Figures 8a and 8d as well as Figures 8b and 8e, although there is substantial variability in the index, enhanced narrowband wave activity is observed before the storms' onset (i.e., before  $t_o - 18$  hr). Moreover, the Pc5 wave activity index increased in the morning sector (from 06:00 to 12:00 UT) for both sets of storms, indicating a wave generation mechanism related to the interaction of the solar wind with backstreaming ion beams upstream of the bow shock (Eastwood et al., 2003; Gary, 1993). Mechanisms generating such narrowband waves also include excitation of magnetospheric waveguide modes by overreflection at the magnetosheath inner boundary (Kivelson & Southwood, 1985; Mann et al., 1999).

### 3.3.4. Global Maps of Pc5 Wave Activity Distribution

In order to further explore the presence of Pc5 wave activity during storms found to be closely related to electron flux enhancements in the storm recovery phase, we divided the selected storms into three phases: pre-onset phase, main phase, and recovery phase based on the *SYM-H* index and the Pc5 wave activity

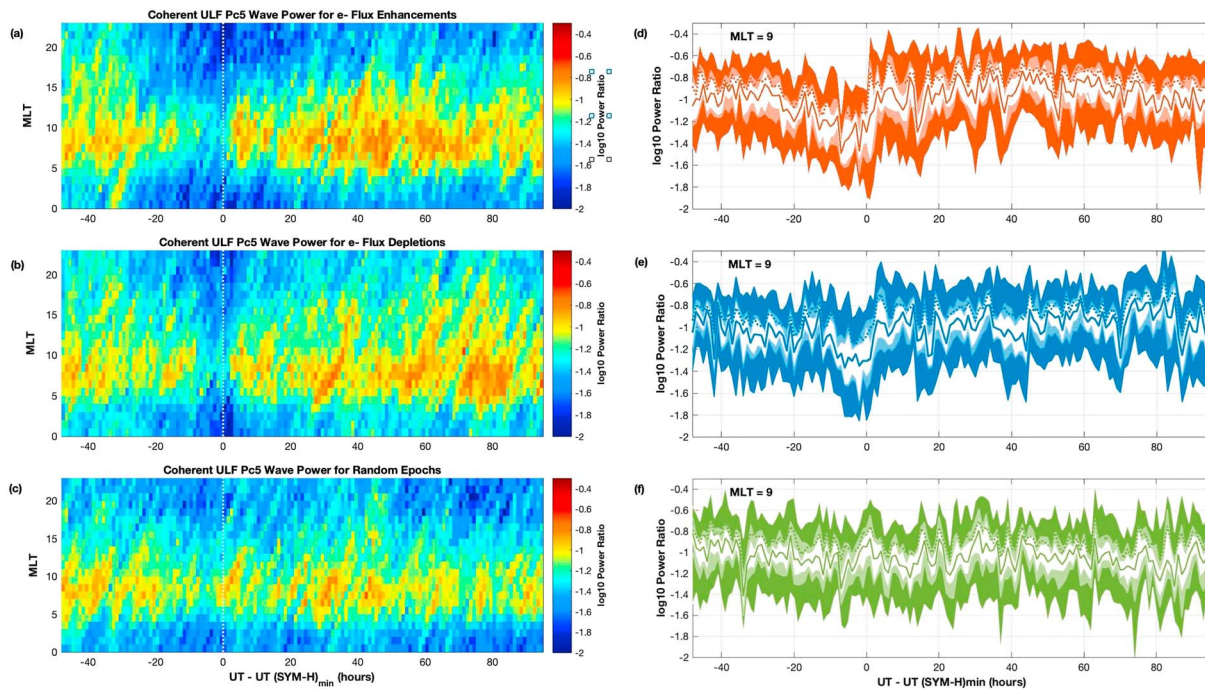


**Figure 8.** Superposed epoch analysis of coherent Pc5 wave power in the north horizontal component for storms leading to electron flux enhancements (a, d), sustained electron flux depletions (b, e), and a set of random epochs (c, f) in the same format as Figure 7. ULF = ultralow frequency; MLT = magnetic local time; UT = Universal Time.

observed in each phase was compared to the corresponding activity of other storms. Since each storm in our list varied in length, this allowed us to look into geomagnetic storm processes contributing to Pc5 wave activity.

Storm onset was defined as the time the *SYM-H* index slope became and stayed negative. Then, we defined the start of the pre-onset phase as the time of the Sudden Storm Commencement. For a number of moderate storms in our list without a clearly defined Sudden Storm Commencement, the start of the pre-onset phase was set 3 hr earlier to the onset of the storm, adopting the definition of Halford et al. (2010). The main phase was identified as the period from the onset of each storm until *SYM-H* reached its minimum value and the slope became positive and, finally, the recovery phase from the end of the main phase until the *SYM-H* index recovered to at least 90% of its prestorm value—only if the *SYM-H* index had not returned to its prestorm value. The specific definition of the recovery phase has been selected to allow time for storm time magnetospheric processes to recede and nonstorm time processes to be once again dominating, which could include the refilling of the plasmasphere (Menk et al., 2014; Song et al., 1988).

Figure 9 shows the median wave power in the Pc5 frequency band across different MLTs and *L* shells ranging from 1 to 10 for each storm phase. Specifically, Figures 9a and 9d show broadband Pc5 wave power before the onset of the 38 storms selected, while Figures 9b and 9e and 9c and 9f from the main and recovery phases of storms. We only consider bins of 1 *L* and 1 hr in MLT that exhibit meaningful difference between the two sets of storms, as confirmed by Kolmogorov-Smirnov testing at a significance level of 5% in each storm phase. As each pair of bins is tested independently, it is likely that the null hypothesis may be falsely rejected. We have, therefore, repeated the comparisons by using a stricter significance level of 3% to find minimal differences in the Kolmogorov-Smirnov test results. Unlike before the storm onset and in the main phase, most pairs of bins with > 150 data points corresponding to the recovery phase were found to reject the null hypothesis; namely, the distribution of data in the bins of storms leading to flux enhancements was not consistent with the distribution of data in the corresponding bins of storms followed by flux depletions. Inlaid polar plots show the total number of data points sampled in each *L* shell and MLT bin.

Before the storm onset, Pc5 wave power was observed enhanced ( $> 10^2$  nT<sup>2</sup>/Hz) in the nightside as well as the dawn sector of the magnetosphere during events that resulted in increased electron fluxes in the recovery phase (Figure 9a). The picture is very different for the main phase, where wave activity is comparable in

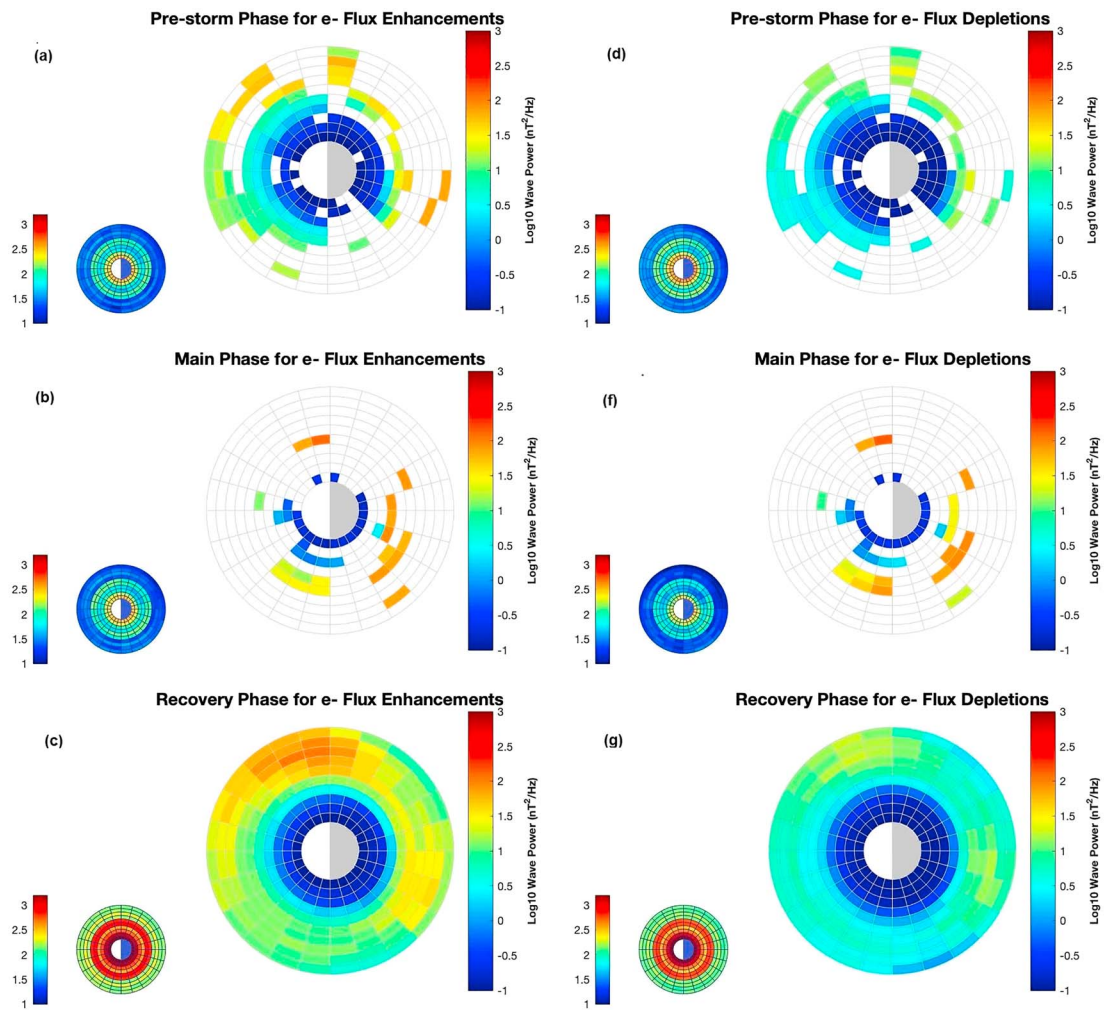


**Figure 9.** Azimuthal and radial distribution of the median of broadband Pc5 wave power in the north horizontal component observed before the onset of storms and during storms' main and recovery phases. (a–c) The power median during storms that led to electron flux enhancements. (d–f) Storms resulting in sustained flux depletions. Inlaid plots show the (log<sub>10</sub> of) number of data points sampled in each *L* shell and magnetic local time bin.

both the nightside and dawn sector among the two sets of storms (Figures 9b and 6e) and higher in the dawn sector for events with sustained electron losses ( $> 10^{2.5}$  nT<sup>2</sup>/Hz over 04:00–08:00 MLT). The relatively low wave activity observed on the duskside, particularly in the recovery phase, may be due to the plasmapause location, which is usually asymmetric and extends further in the duskside where the dayside bulge surges sunward to form a broad plume after the initial erosion of the plasmasphere (Chappell et al., 1971; Goldstein & Sandel, 2005).

Figure 10 shows that the distribution of coherent Pc5 wave power peaks in the morning sector (06:00–12:00 MLT) during all three phases of storms leading to electron flux enhancements (Figures 10a–10c) and sustained depletions (Figures 10d–10f). We should note the pronounced peak in the outer magnetosphere from *L* shell 5 to 10 (Figures 10c and 10f), partly consistent with the results of previous ground-based studies suggesting that narrowband Pc5 waves dominate in the prenoon dayside during the storm recovery phase, when particle injections recede (Posch et al., 2003). The studies of Engebretson et al. (1998) and Rae et al. (2012) also suggest that such ULF waves are generated by a physical mechanism related to the velocity shear between the solar wind and the magnetopause—they are shear mode Pc5 waves. Enhanced wave activity in the dayside is likely associated with additional physical processes, including solar wind dynamic pressure variability (as seen in Figures 2c and 2g).

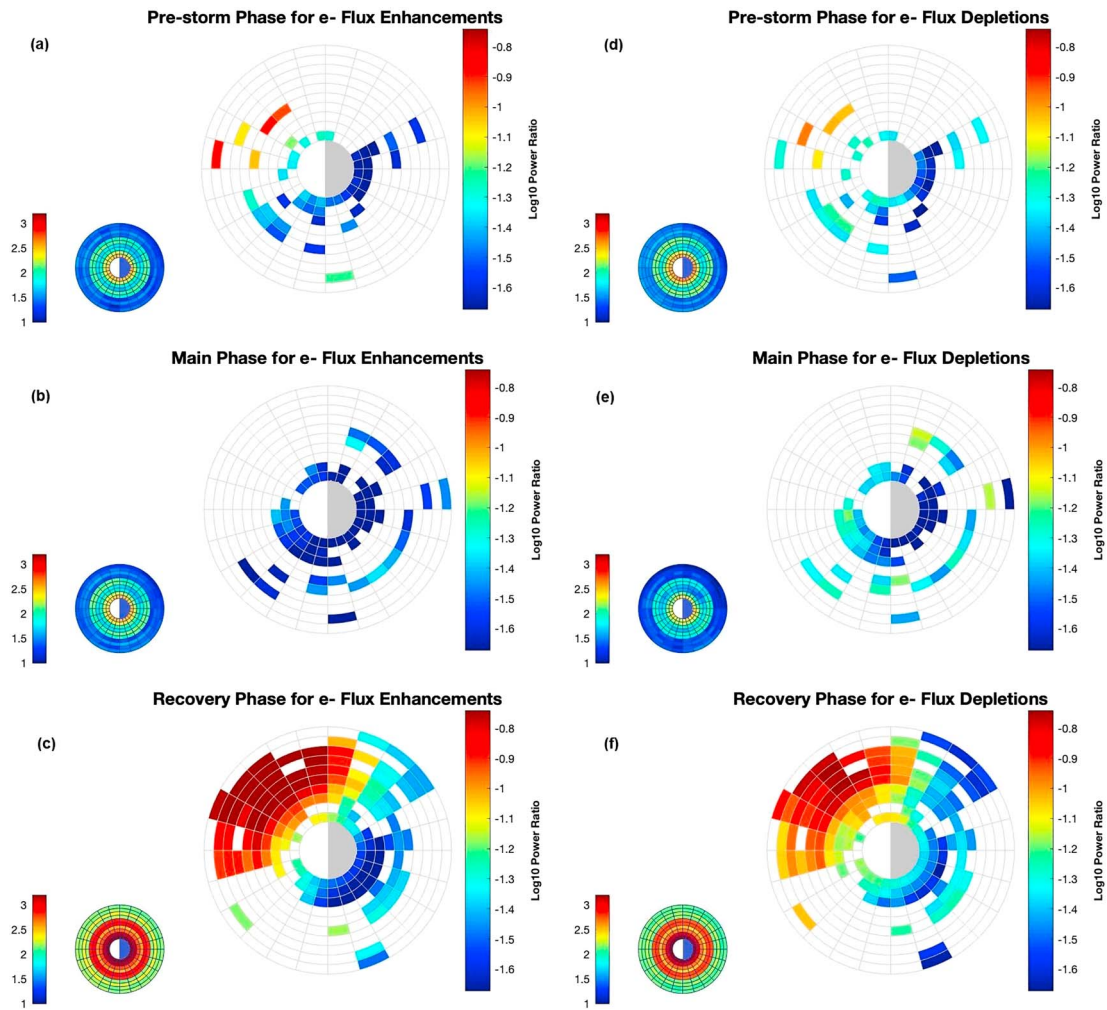


**Figure 10.** Azimuthal and radial distribution of the median of coherent Pc5 wave power before the onset of storms and during storms' main and recovery phases. (a–c) The index median during storms that led to electron flux enhancements. (d–f) Storms resulting in sustained flux depletions. Inlaid plots show the (log10 of) number of data points sampled in each  $L$  shell and magnetic local time bin.

#### 4. Discussion

Our results, using a more comprehensive data set for Pc5 wave power measured from ground magnetometers, confirm previous studies on the occurrence of wave activity with respect to storms (Engebretson et al., 1998; Posch et al., 2003) and storm time radiation belt dynamics. Specifically, in half of the magnetic storms of the previous solar cycle 23 investigated (19 out of 38 storms), there was rapid depletion of relativistic electron fluxes followed by an increase by orders of magnitude on hour timescales during the recovery of most intense storms. The response of the outer radiation belt electrons to transient solar wind streams (i.e., CMEs) was in other cases (19 storms) different with the fast depletion of relativistic electron fluxes in the main phase being sustained throughout the recovery phase. This difference in the response of the outer radiation belt to storms could partly be explained by enhanced ULF Pc5 wave activity associated with higher solar wind flow speed in the recovery phase of storms leading to enhanced electron fluxes, which is consistent with results of geosynchronous (O'Brien et al., 2001, 2003) as well as high elliptical orbit data studies (Mann et al., 2004) and modeling (Elkington et al., 2003). Mann et al. (2004) found that megaelectron volt electron fluxes respond first at the geosynchronous orbit at the outskirts of the outer radiation belt before subsequently peaking at lower  $L$  shells. This could account for solar wind speed or ULF Pc5 wave power-correlated acceleration processes that operate by inward radial transport.

We found that the, on average, twofold increase in relativistic electron fluxes, observed by GOES satellites at geosynchronous orbit and a broad range of  $L$  shells by the SAMPEX satellite, was related to enhanced Pc5 wave

activity. The square root of PSD in the Pc5 frequency range generally started to increase as early as  $t_0 - 24$  hr and remained at values  $> 10^{1.2}$  nT<sup>2</sup>/Hz until  $t_0 + 62$  hr in the recovery phase, significantly longer than in storms leading to sustained electron flux depletions where PSD was reduced to values  $< 10^{1.2}$  nT<sup>2</sup>/Hz at  $t_0 + 8$  hr on average (Figures 4a and 4b). During this time, the relativistic electron fluxes were increased (Figures 1d and 1e), suggesting that ULF waves had a role to play in electron acceleration and contributed to the reformation of the outer radiation belt. This correlation supports indirectly the scenario of diffusive radial transport—a slow process acting as the square root of time (Elkington et al., 2003). On the other hand, the presence of coherent, narrowband Pc5 waves in storms' recovery phase (Figures 5a and 5b) can accelerate electrons through drift resonance (Degeling et al., 2008) and a relationship to time is also expected, challenging the standard paradigm for transport on the drift motion timescale being diffusive in nature (Mann et al., 2013).

Our calculation of Pc5 wave power and our Pc5 wave activity index differs in some important aspects from the previous studies examining ULF waves. Relative to Engebretson et al. (1998), Mathie & Mann, (2000, 2001, O'Brien et al. (2001), O'Brien et al. (2003), and Posch et al. (2003), we have calculated the wavelet scale-averaged PSD over  $L$  shells ranging from 1 to 10 and MLT between 00:00 and 23:59, which would not have been possible if measurements from a single ground magnetometer network had been used. Our results are, therefore, not directly comparable to the findings of these and other ground-based studies; we have identified in our data wave activity that originated almost simultaneously from many different regions of both the dayside and nightside magnetosphere instead of a single one. However, comparison of our superposed epoch of Pc5 wave power and Pc5 wave activity index over all MLTs and a wide range of  $L$  shells confirms that the peak of Pc5 wave activity is observed about the *SYM-H* index minimum and of narrowband Pc5 wave activity in the recovery phase after having drastically dropped off in the main phase of storms.

Broadband Pc5 wave power was also found to be concentrated at higher  $L$  shells during all storm phases (Figures 4a and 4b), reinforcing the findings of Georgiou et al. (2015). The gradual decay of power with decreasing  $L$  shell is likely associated with an external source of Pc5 waves in the solar wind rather than an internal one. Solar wind-driven waves with frequencies in the Pc5 frequency band may not penetrate deep into the magnetosphere (Loto'aniu et al., 2006). According to Hartinger et al. (2010) and Balasis et al. (2015), it is possible that nominal conditions in the plasmasphere are not conducive to magnetohydrodynamics resonances in the Pc5 frequency band. If fundamental FLR and cavity resonance frequencies are not in the Pc5 frequency band, the average power will be low in the plasmasphere. In our study, the depth of power penetration (to as slow as  $L$  shell  $< 2$ ) appeared to be well correlated with the minimum *SYM-H* index of each storm, similar to the penetration of relativistic electron flux of the outer radiation belt (Figures 6a and 6b). In addition, the  $L$  shell where the power peak is observed is closely related to the plasmopause location, as seen in both storms leading to electron flux enhancements and prolonged depletions.

Power at millihertz frequencies is produced by a number of physical processes, including externally generated processes such as shear instabilities at the flanks (Claudepierre et al., 2008) or compressive variations in the solar wind dynamic pressure (Kepko et al., 2002) with small azimuthal wave numbers ( $m \leq 10$ ) and internally generated waves induced by ring current plasma instabilities with  $m = 40-120$  (Rae et al., 2007). Fluctuations in the solar wind velocity and/or dynamic pressure at Pc5 frequencies can also contribute to the variability observed at similar frequencies in the geomagnetic field. Sometimes, the same frequencies are observed over a broad range of latitudes (Samson & Rostoker, 1972). Storm time Pc5 waves generated by injected ions that have been excited by kinetic drift instabilities in the ring current can be narrow band but are not detectable in ground magnetometer measurements (Hughes & Southwood, 1976). During storms, these are observed in space toward dusk (Hudson et al., 2004). Figures 8a and 8b show that narrowband Pc5 wave power concentrated in the prestorm phase as well as the storm recovery phase supports additional redistribution of radiation belt electron flux under the action of broadband Pc5 waves (Mann et al., 2013). In accordance with the findings of Nosé et al. (1995), Engebretson et al. (1998), and Posch et al. (2003) in ground-based and spaceborne measurements, they exhibit maximum occurrence and amplitude in the dawn-noon sector (05:00 to 14:00 MLT of Figures 8a and 8b).

In the superposed epoch analysis, we had an overlap between the pre-onset and main phases of storms of different duration as well as between the recovery phase and the pre-onset of the next storm. With the individual storm phases defined, there were not different storm phases overlapping with each other as well as with relatively quiet periods. Nonetheless, the overall distribution of broadband and narrowband Pc5 wave power across MLTs and  $L$  shells has not changed in Figures 9 and 10. The peak of the median Pc5 wave power

still remained in the main phase of the storm but appears higher during the main phase of those events that did not produce relativistic electrons. Epoch time bins partly covered both pre-onset and main phases, and therefore, Pc5 wave power observed at different storm phases may have been averaged out.

The statistical comparison of Pc5 wave power observed during storms followed by either an increase in the  $E > 1.5$  MeV electron fluxes or a sustained depletion, presented here and previous studies, demonstrated the importance of magnetospheric conditions in understanding and subsequently predicting the response of the outer radiation belt. Simms et al. (2014) argued that the electron flux response could be modeled by a set of parameters of which Pc5 wave power has the highest predictive ability. Intense and persistent Pc5 wave activity has also been shown to lead to enhanced fluxes of relativistic electrons within 1 to 2 days (Mann et al., 2004). Pc5 waves generated in response to solar wind excitation—in particular, increased  $V_{sw}$  (Figures 2b and 2f)—could serve as intermediary between solar wind and radiation belts' electron population. The development and propagation of such geomagnetic pulsations are, however, profoundly influenced by the magnetosphere's structure in terms of both magnetic field and plasma characteristics. Engebretson et al. (1998) argued that it is difficult to make estimates of Pc5 wave power on the basis of  $V_{sw}$  alone. On the contrary, one must consider physical characteristics intrinsic to the solar wind or related to its interaction with the Earth's magnetosphere.

Distortion or inward progression of the plasmopause during the course of storms is expected to gradually alter wave properties and subsequently observations of wave power. Similarly, near-tail dynamics are seen to be of importance, such as the varying plasma sheet populations providing low-energy (10 to 100 keV) electrons that plays a key role in radiation belt dynamics. Two solar wind parameters are known to be related to the plasma sheet number density: the north-south component of IMF ( $B_z$  component, shown in Figures 2a and 2e) and solar wind number density (Figures 2d and 2h). The solar wind number density correlates with the plasma sheet number density positively (Borovsky et al., 1998), remaining at higher values during storms producing relativistic electrons. Surprisingly, the plasma sheet electron density response to southward IMF is also positive (Dubyaagin et al., 2016).

Additional magnetospheric processes have been shown to be critical in radiation belt dynamics. Substorm particle injections are thought to be a major contributor to increases of the total electrons content. Rather than injecting megaelectron volt particles into the outer radiation belt, substorm activity provides a low-energy seed population of kiloelectron volt particles that are subsequently accelerated to higher energies (Fok et al., 2001). Forsyth et al. (2016) found that substorms are followed by increases with time lag of 1–3 days, namely, comparable to the time lag between  $V_{sw}$  and the response of relativistic electrons in the outer radiation belt (Lyatsky & Khazanov, 2008; Mann et al., 2004). In Figures 1d and 1e, relativistic electron fluxes have recovered to their average prestorm level  $\approx 1$  day after the *SYM-H* minimum—if they recovered at all—and reached their highest value  $\approx 2.3$  days after the  $V_{sw}$  maximum (Figure 2b). Similar to the enhancement of Pc5 wave power, the frequency of substorms depends on  $V_{sw}$ , as Newell et al. (2016) have argued.

Besides the effect of substorms, enhanced magnetospheric convection acts to enhance and maintain seed electron populations—plasma sheet particles transported earthward by tail processes which can be accelerated via wave-particle interactions with whistler mode chorus (Kissinger et al., 2014; Rodger et al., 2016). In particular, Kissinger et al. (2014) have found that storms with long-duration intervals of enhanced convection without any substorm expansions in the recovery phase are more likely to increase relativistic electron fluxes in the outer radiation belt than storms without quasi-steady convection. In turn, magnetospheric convection triggers enhancement of chorus wave activity. This result differs from Rodger et al. (2016) who found repetitive substorm onsets associated with enhancements in the flux of relativistic electrons, probably due to enhanced chorus activity driven by magnetospheric convection. In this context, our results suggest enhanced Pc5 wave activity in the recovery phase that could, however, act as a proxy for an acceleration mechanism other than inward radial diffusion leading to enhancements of relativistic electron fluxes in the outer radiation belt.

## 5. Conclusions

Along with solar wind conditions leading to the onset of magnetic storms followed by sustained depletions or an increase in relativistic electron fluxes in the outer radiation belt relativistic electron, this study investigated the spatial and temporal profiles of ULF Pc5 wave power based on measurements from more than 180 ground magnetometers of SuperMAG. One limitation of similar efforts in the past had been the limited observations of ULF Pc5 wave activity originating from the outskirts of the magnetosphere and penetrating deep into the

inner magnetosphere with continuity in space and time. Using ground magnetometer data from the virtual network of SuperMAG, we found the following:

- The imprint of narrowband Pc5 waves particularly pronounced in the morning (from 06:00 to 12:00 MLT) sector of the magnetosphere and more broadband Pc5 waves in the premidnight (from 18:00 to 24:00 MLT) or dawn (from 03:00 to 09:00 MLT) sector, depending on the storm phase;
- Enhanced Pc5 wave activity penetrating to low  $L$  shells ( $< 4L$ ) and sustained throughout the recovery phase of storms (on average 62 hr after the  $SYM-H$  index minimum) followed by increases in  $1.5 < E < 6$ -MeV electron fluxes observed in the outer radiation belt;
- The depth of wave activity penetration (to as low  $L < 2$ ) associated with the intensity of each storm quantified by the minimum  $SYM-H$ , similar to the penetration of relativistic electron flux in the outer radiation belt;
- The response of the outer belt electron fluxes to the selected storms related to the level of geomagnetic activity as well as to solar wind driving. A minimum time interval of southward IMF  $B_z$  component as well as high solar wind speed in the recovery phase of storms was a necessary condition for enhanced electron fluxes in the storm recovery phase; high levels of solar wind density and dynamic pressure was not necessary;
- The outer radiation belt to respond in two different ways, relativistic electron fluxes were either enhanced or depleted, depending on a combination rather than individual IMF and solar wind parameters which was proposed by Borovsky and Birn (2014) to quantify the magnetic reconnection at the dayside magnetopause affecting multiple magnetospheric processes.

Our statistical results are important in characterizing Pc5 wave activity which, in turn, sheds light on the solar wind-magnetosphere interaction as well as on energetic particle transport. The set of storms selected reveals that solar wind conditions alone do not define the different responses in outer radiation belt electron fluxes, and ULF pulsations have a role to play. Nonetheless, magnetic field measurements alone cannot fully characterize all features of ULF pulsations and electric field measurements are required to provide an unambiguous picture of ULF wave activity in both the inner and outer magnetosphere. Owing to the spatial coverage of ground magnetometers, the distribution of Pc5 wave power in local time and  $L$  shell could be studied in detail. In future studies, we intend to use both electric and magnetic field data from multiple spacecraft to compare Pc5 wave activity at different  $L$  shells during the course of storms.

## References

- Akasofu, S.-I. (1991). Interplanetary energy flux associated with magnetospheric substorms. *Planetary and Space Science*, 27, 425–431.
- Baker, D. N., Jaynes, A. N., Kanekal, S. G., Foster, J. C., Erickson, P. J., Fennell, J. F., et al. (2016). Highly relativistic radiation belt electron acceleration, transport, and loss: Large solar storm events of March and June 2015. *Journal of Geophysical Research: Space Physics*, 121, 6647–6660. <https://doi.org/10.1002/2016JA022502>
- Baker, D. N., Jaynes, A. N., Li, X., Henderson, M. G., Kanekal, S. G., Reeves, G. D., et al. (2014). Gradual diffusion and punctuated phase space density enhancements of highly relativistic electrons: Van Allen Probes observations. *Geophysical Research Letters*, 41, 1351–1358. <https://doi.org/10.1002/2013GL058942>
- Balasis, G., Daglis, I. A., Georgiou, M., Papadimitriou, C., & Haugmans, R. (2013). Magnetospheric ULF wave studies in the frame of Swarm mission: A time-frequency analysis tool for automated detection of pulsations in magnetic and electric field observations. *Earth, Planets and Space*, 65, 1385–1389.
- Balasis, G., Daglis, I. A., Mann, I. R., Papadimitriou, C., Zesta, E., Georgiou, M., et al. (2015). Multi-satellite study of the excitation of Pc3 and Pc4-5 ULF waves and their penetration across the plasmopause during the 2003 Halloween superstorm. *Annales Geophysicae*, 19, 1237–1252.
- Balasis, G., Daglis, I. A., Zesta, E., Papadimitriou, C., Georgiou, M., Haugmans, R., & Tsinganos, K. (2012). ULF wave activity during the 2003 Halloween superstorm: Multipoint observations from CHAMP, Cluster and Geotail missions. *Annales Geophysicae*, 30, 1751–1768.
- Blake, J. B., Kolasinski, W. A., Fillius, R. W., & Mullen, E. G. (1992). Injection of electrons and protons with energies of tens of MeV into  $L < 3$  on March 24, 1991. *Geophysical Research Letters*, 19(8), 821–824.
- Borovsky, J. E., & Birn, J. (2014). The solar wind electric field does not control the dayside reconnection rate. *Journal of Geophysical Research: Space Physics*, 119, 751–760. <https://doi.org/10.1002/2013JA019193>
- Borovsky, J. E., Thomsen, M. F., & Elphic, R. C. (1998). The driving of the plasma sheet by the solar wind. *Journal of Geophysical Research*, 103, 17, 617–17, 639.
- Boyd, A. J., Turner, D. L., Reeves, G. D., Spence, H. E., Baker, D. N., & Blake, J. B. (2018). What causes radiation belt enhancements: A survey of the Van Allen Probes era. *Geophysical Research Letters*, 45, 5253–5259. <https://doi.org/10.1029/2018GL077699>
- Brautigam, D. H., & Albert, J. M. (2000). Radial diffusion analysis of outer radiation belt electrons during the October 9, 1990, magnetic storm. *Journal of Geophysical Research*, 105(A1), 291–309.
- Chappell, C. R., Harris, K. K., & Sharp, G. W. (1971). The dayside of the plasmasphere. *Journal of Geophysical Research*, 76, 7632–7647.
- Chen, Y., Reeves, G. D., & Friedel, R. H. W. (2007). The energization of relativistic electrons in the outer Van Allen radiation belt. *Nature Communications*, 3, 614–617.
- Claudepierre, S. G., Elkington, S. R., & Wiltberger, M. (2008). Solar wind driving of magnetospheric ULF waves: Pulsations driven by velocity shear at the magnetopause. *Journal of Geophysical Research*, 113, A05218. <https://doi.org/10.1029/2007JA012890>
- Cook, W. R., Cummings, A. C., Cummings, J. R., Garrard, T. L., Kecman, B., Mewaldt, R. A., et al. (1996). PET: A proton/electron telescope for studies of magnetospheric, solar, and galactic particles. *IEEE Transactions on Geoscience and Remote Sensing*, 31, 565–571.

## Acknowledgments

Part of the work leading to this paper received funding by NERC grant NE/P017185/1. I. J. R. was supported by STFC grant ST/N000722/1 and NERC grant NE/P017185/1. For the ground magnetometer data used in this study, we gratefully acknowledge the following people and organizations: Intermagnet; USGS, J. J. Love; CARISMA, PI I. R. Mann; CANMOS; the S-RAMP database, PI K. Yumoto and K. Shiokawa; the SPIDR database; AARI, PI O. Troshichev; the MACCS programme, PI M. Engebretson, Geomagnetism Unit of the Geological Survey of Canada; GIMA; MEASURE, UCLA IGPP and Florida Institute of Technology; SAMBA, PI E. Zesta; 210 MM Chain, PI K. Yumoto; SAMNET, PI F. Honary; the institutes who maintain the IMAGE magnetometer array, PI E. Tanskanen; PENGUIN; AUTUMN, PI M. Connors; DTU Space, PI J. Matzka; South Pole and McMurdo Magnetometer, PI S. L. J. Lanzarotti and A. T. Weatherwax; ICESTAR; RAPIDMAG; British Antarctic Survey; Mc-Mac, PI P. Chi; BGS, PI S. Macmillan; Pushkov Institute of Terrestrial Magnetism, Ionosphere and RadioWave Propagation (IZMIRAN); GFZ, PI J. Matzka; MFGI, PI B. Heilig; IGFAPAS, PI J. Reda; University of L'Aquila, PI M. Vellante; ENIGMA, PI G. Balasis and I. A. Daglis; and SuperMAG, PI J. W. Gjerloev. All ground magnetometer data can be accessed through the SuperMAG data service at <http://supermag.jhuapl.edu/>. We also acknowledge the following sources of additional data: the Kyoto WDC for Geomagnetism and the observatories that produce and make AE and  $SYM-H$  indices available at <http://wdc.kugi.kyoto-u.ac.jp/>, SPDF CDAWeb and the science teams that provided interplanetary data through <http://cdaweb.gsfc.nasa.gov/>, NOAA's Space Environment Center at <http://www.ngdc.noaa.gov/stp/satellite/goes/>, and the Johns Hopkins University's Applied Physics Laboratory teams for energetic particle data made available at <http://www.srl.caltech.edu/sampex/>.

- Degeling, A. W., Ozeke, L. G., Rankin, R., Mann, I. R., & Kabin, K. (2008). Drift resonant generation of peaked relativistic electron distributions by ULF Pc5 waves. *Journal of Geophysical Research*, *113*, A02208. <https://doi.org/10.1029/2007JA012411>
- Degeling, A. W., & Rankin, R. (2008). Resonant drift echoes in electron phase space density produced by dayside Pc5 waves following a geomagnetic storm. *Journal of Geophysical Research*, *113*, A10220. <https://doi.org/10.1029/2008JA013254>
- Dubyagin, S., Ganushkina, N. Y., Sillanpää, I., & Runov, A. (2016). Solar wind driven variations of electron plasma sheet densities and temperatures beyond geostationary orbit during storm times. *Journal of Geophysical Research: Space Physics*, *121*, 8343–8360. <https://doi.org/10.1002/2016JA022947>
- Dungey, J. W. (1961). Interplanetary magnetic field and the auroral zones. *Physical Review Letters*, *6*, 47–48.
- Eastwood, J. P., Balogh, A., Lucek, E. A., Mazelle, C., & Dandouras, I. (2003). On the existence of Alfvén waves in the terrestrial foreshock. *Annales Geophysicae*, *21*, 1457–1465.
- Echer, E., Gonzalez, W. D., Tsurutani, B. T., & Gonzalez, A. L. C. (2008). Interplanetary conditions causing intense magnetic storm (Dst  $\leq$  -100 nt) during solar cycle 23 (1996 – 2006). *Journal of Geophysical Research*, *113*, A05221. <https://doi.org/10.1029/2007JA012744>
- Elkington, S. R., Hudson, M. K., & Chan, A. A. (2003). Resonant acceleration and diffusion of outer zone electrons in an asymmetric geomagnetic field. *Journal of Geophysical Research*, *108*(A3), 2156–2202. <https://doi.org/10.1029/2001JA009202>
- Engebretson, M., Glassmeier, K.-H., Stellmacher, M., Hughes, W. J., & Lühr, H. (1998). The dependence of high-latitude Pc5 wave power on solar wind velocity and on the phase of high-speed solar wind streams. *Journal of Geophysical Research*, *103*(A11), 26,271–26,283.
- Fälthammar, C.-G. (1965). Effects of time dependent electric fields on geomagnetically trapped radiation. *Journal of Geophysical Research*, *70*, 2503–2516.
- Fälthammar, C.-G. (1968). Radial diffusion by violation of the third adiabatic invariant. In B. M. McCormac (Ed.), *Earth's particles and fields* (pp. 157). Reinhold, New York: NATO Advanced Study Institute.
- Fei, Y., Chan, A. A., Elkington, S. R., & Wiltberger, M. J. (2006). Radial diffusion and MHD particle simulations of relativistic electron transport by ULF waves in the September 1998 storm. *Journal of Geophysical Research*, *111*, A12209. <https://doi.org/10.1029/2005JA011211>
- Fok, M.-C., Moore, T. E., & Spjeldvik, W. N. (2001). Rapid enhancement of radiation belt electron fluxes due to substorm dipolarization of the geomagnetic field. *Journal of Geophysical Research*, *106*(A3), 3873–3881.
- Forsyth, C., Rae, I. J., Murphy, K. R., Freeman, M. P., Huang, C.-L., Spence, H. E., et al. (2016). What effect do substorms have on the content of the radiation belts? *Journal of Geophysical Research: Space Physics*, *121*, 6292–6306. <https://doi.org/10.1002/2016JA022620>
- Gary, S. P. (1993). *Theory of space plasma microinstabilities*. New York: Cambridge University Press.
- Georgiou, M., Daglis, I. A., Zesta, E., Balasis, G., Mann, I. R., Katsavrias, C., & Tsinganos, K. (2015). Association of radiation belt electron enhancements with earthward penetration of Pc5 ULF waves: A case study of intense 2001 magnetic storms. *Annales Geophysicae*, *33*, 1431–1442.
- Gjerloev, J. W. (2009). A global ground-based magnetometer initiative. *Eos, Transactions American Geophysical Union*, *90*, 230–231.
- Goldstein, J., & Sandel, B. R. (2005). The global pattern of evolution of plasmaspheric drainage plumes. In J. Burch, M. Schulz, & H. Spence (Eds.), *Inner magnetosphere interactions: New perspectives from imaging* (Vol. 159, pp. 1). Washington, DC: American Geophysical Union.
- Gopalswamy, N., Yashiro, S., Michalek, G., Stenborg, G., Vourlidas, A., Freeland, S., & Howard, R. (2009). The SOHO/LASCO CME catalog. *Earth, Moon, and Planets*, *104*, 295–313.
- Green, J. C., & Kivelson, M. G. (2004). Relativistic electrons in the outer radiation belt: Differentiating between acceleration mechanisms. *Journal of Geophysical Research*, *109*, A03213. <https://doi.org/10.1029/2003JA010153>
- Halford, A. J., Fraser, B. J., & Morley, S. K. (2010). EMIC wave activity during geomagnetic storm and non-storm periods. *Journal of Geophysical Research*, *115*, A12248. <https://doi.org/10.1029/2010JA015716>
- Harteringer, M., Moldwin, M. B., Angelopoulos, V., Takahashi, K., Singer, H. J., Anderson, R. R., et al. (2010). Pc5 wave power in the quiet-time plasmasphere and trough: CRRES observations. *Geophysical Research Letters*, *37*, L07107. <https://doi.org/10.1029/2010GL042475>
- Hendry, A. T., Rodger, C. J., Clilverd, M. A., Thomson, N. R., Morley, S. K., & Raita, T. (2005). Rapid radiation belt losses occurring during high-speed solar wind stream-driven storms: Importance of energetic electron precipitation. In D. Summers, et al. (Eds.), *Dynamics of the Earth's radiation belts and inner magnetosphere* (Vol. 199, pp. 213–224). Wiley: American Geophysical Union.
- Hietala, E. K. J., Hietala, H., Turner, D. L., Koskinen, H. E. J., Pulkkinen, T. I., Rodriguez, J. V., et al. (2015). Unraveling the drivers of the storm time radiation belt response. *Geophysical Research Letters*, *42*, 3076–3084. <https://doi.org/10.1002/2015GL063542>
- Horne, R. B., Horne, R. M., Shprits, Y. Y., Meredith, N. P., Glauert, S. A., Smith, A. J., et al. (2005). Wave acceleration of electrons in the Van Allen radiation belts. *Nature*, *437*, 227–230.
- Huang, C.-L., Spence, H. E., Singer, H. J., & Hughes, W. J. (2010). Modeling radiation belt radial diffusion in ULF wave fields: 1. Quantifying ULF wave power at geosynchronous orbit in observations and in global MHD model. *Journal of Geophysical Research*, *115*, A06215. <https://doi.org/10.1029/2009JA014917>
- Hudson, M. K., Baker, D. N., Goldstein, J., Kress, B. T., Paral, J., Toffoletto, F. R., & Wiltberger, M. (2014). Simulated magnetopause losses and Van Allen probe flux dropouts. *Geophysical Research Letters*, *41*, 1113–1118. <https://doi.org/10.1002/2014GL059222>
- Hudson, M. K., Denton, R. E., Lessard, M. R., Miftakhova, E. G., & Anderson, R. R. (2004). A study of Pc5 ULF oscillations. *Annales Geophysicae*, *22*, 289–302.
- Hughes, W. J., & Southwood, D. J. (1976). The screening of micropulsation signals by the atmosphere and the ionosphere. *Journal of Geophysical Research*, *81*(19), 3234–3240.
- Iles, R. H. A., Fazakerley, A. N., Johnstone, A. D., Meredith, N. P., & Bhler, P. (2002). The relativistic electron response in the outer radiation belt during magnetic storms. *Annales Geophysicae*, *20*, 957–965.
- Jacobs, J. A., Kato, Y., Matsushita, S., & Troitskaya, V. A. (1964). Classification of geomagnetic micropulsations. *Journal of Geophysical Research*, *69*, 180.
- Katsavrias, C., Daglis, I. A., Turner, D. L., Sandberg, I., Papadimitriou, C., Georgiou, M., & Balasis, G. (2015). Nonstorm loss of relativistic electrons in the outer radiation belt. *Geophysical Research Letters*, *42*, 10,521–10,530. <https://doi.org/10.1002/2015GL066773>
- Kellerman, A. C., & Shprits, Y. Y. (2012). On the influence of solar wind conditions on the outer-electron radiation belt. *Journal of Geophysical Research*, *117*, A05217. <https://doi.org/10.1029/2011JA017253>
- Kellogg, P. J. (1959). Van Allen radiation of solar origin. *Nature*, *183*, 1295–1297.
- Kepko, L., Spence, H. E., & Singer, H. J. (2002). ULF waves in the solar wind as direct drivers of magnetospheric pulsations. *Geophysical Research Letters*, *29*(8), 1197. <https://doi.org/10.1029/2001GL014405>
- Kim, K. C., Lee, D. Y., Kim, H.-J., Lyons, L. R., Lee, E. S., Ozturk, M. K., & Choi, C. R. (2008). Numerical calculations of relativistic electron drift loss effect. *Journal of Geophysical Research*, *113*, A09212. <https://doi.org/10.1029/2007JA013011>

- Kissing, J., Kepko, L., Baker, D. N., Kanekal, S., McPherron, R. L., & Angelopoulos, V. (2014). The importance of storm time steady magnetospheric convection in determining the final relativistic electron flux level. *Journal of Geophysical Research: Space Physics*, *119*, 7433–7443. <https://doi.org/10.1002/2014JA019948>
- Kivelson, M. G., & Southwood, D. J. (1985). Resonant ULF waves: A new interpretation. *Geophysical Research Letters*, *12*, 49–52.
- Kozyreva, O., Pilipenko, V., Engebretson, M. J., Yumoto, K., Watermann, J., & Romanova, N. (2007). In search of a new ULF wave index: Comparison of Pc5 power with dynamics of geostationary relativistic electrons. *Planetary and Space Science*, *55*, 755–769.
- Lepping, R. P., Berdichevsky, D. B., Wu, C.-C., Szabo, A., Narock, T., Mariani, F., et al. (2006). A summary of WIND magnetic clouds for years 1995–2003: Model-fitted parameters, associated errors and classifications. *Annales Geophysicae*, *24*, 215–245.
- Li, X., Baker, D. N., Temerin, M., Reeves, G. D., Friedel, R., & C., Shen (2005). Energetic electrons, 50 keV to 6 MeV, at geosynchronous orbit: Their responses to solar wind variations. *Space Weather*, *3*, S04001. <https://doi.org/10.1029/2004SW000105>
- Li, X., Roth, I., Temerin, M., Wygant, J. R., Hudson, M. K., & Blake, J. B. (1993). Simulation of the prompt energization and transport of radiation belt particle during the March 24, 1991 SSC. *Geophysical Research Letters*, *20*, 2423–2426.
- Li, L. Y., Yu, J., Cao, J. B., Yang, J. Y., Li, X., Baker, D. N., et al. (2017). Roles of whistler mode waves and magnetosonic waves in changing the outer radiation belt and the slot region. *Journal of Geophysical Research: Space Physics*, *122*, 5431–5448. <https://doi.org/10.1002/2016JA023634>
- Liu, W., Sarris, T. E., Li, X., Elkington, S. R., Ergun, R., Angelopoulos, V., et al. (2009). Electric and magnetic field observations of Pc4 and Pc5 pulsations in the inner magnetosphere: A statistical study. *Journal of Geophysical Research*, *114*, A12206. <https://doi.org/10.1029/2009JA014243>
- Liu, W., Sarris, T. E., Li, X., Ergun, R., Angelopoulos, V., Bonnell, J., & Glassmeier, K. H. (2010). Solar wind influence on Pc4 and Pc5 ULF wave activity in the inner magnetosphere. *Journal of Geophysical Research*, *115*, A12201. <https://doi.org/10.1029/2010JA015299>
- Loto'aniu, T. M., Mann, I. R., Ozeke, L. G., Chan, A. A., Dent, Z. C., & Milling, D. K. (2006). Radial diffusion of relativistic electrons into the radiation belt slot region during the 2003 Halloween geomagnetic storms. *Journal of Geophysical Research*, *111*, A04218. <https://doi.org/10.1029/2005JA011355>
- Loto'aniu, T. M., Singer, H. J., Waters, C. L., Angelopoulos, V., Mann, I. R., Elkington, S. R., & Bonnell, J. W. (2010). Relativistic electron loss due to ultra-low frequency waves and enhanced outward radial diffusion. *Journal of Geophysical Research*, *115*, A12245. <https://doi.org/10.1029/2010JA015755>
- Lyatsky, W., & Khazanov, G. V. (2008). Effect of geomagnetic disturbances and solar wind density on relativistic electrons at geostationary orbit. *Journal of Geophysical Research*, *113*, A08224. <https://doi.org/10.1029/2008JA013048>
- Lyons, L. R., Zesta, E., Xu, Y., Sánchez, E. R., Samson, J. C., Reeves, G. D., et al. (2002). Auroral poleward boundary intensifications and tail bursty flows: A manifestation of a large-scale ULF oscillation? *Journal of Geophysical Research*, *107*(A11), 1352. <https://doi.org/10.1029/2001JA000242>
- Mann, I. R., Lee, E. A., Claudepierre, S. G., Fennell, J. F., Degeling, A., Rae, I. J., et al. (2013). Discovery of the action of a geophysical synchrotron in the Earth's Van Allen radiation belts. *Nature Communications*, *4*, 2795.
- Mann, I. R., O'Brien, T. P., & Milling, D. K. (2004). Correlations between ULF wave power, solar wind speed and relativistic electron flux in the magnetosphere: Solar cycle dependence. *Journal of Atmospheric and Solar-Terrestrial Physics*, *66*(2), 187–198.
- Mann, I. R., Wright, A. N., Mills, K., & Nakariakov, V. M. (1999). Excitation of magnetospheric waveguide modes by magnetosheath flows. *Journal of Geophysical Research*, *104*, 333–353.
- Mathie, R. A., & Mann, I. R. (2000). A correlation between extended intervals of ULF wave power and storm-time geosynchronous relativistic electron flux enhancements. *Geophysical Research Letters*, *27*, 3261–3264.
- Mathie, R. A., & Mann, I. R. (2001). On the solar wind control of Pc5 ULF pulsation power at mid-latitudes: Implications for MeV electron acceleration in the outer radiation belt. *Journal of Geophysical Research*, *106*, 29,783–29,796.
- Menk, F. W., Kale, Z., Sciffer, M., Robinson, P., Waters, C., Grew, R., et al. (2014). Remote sensing the plasmasphere, plasmopause, plumes and other features using ground-based magnetometers. *Journal of Space Weather and Space Climate*, *4*, A34.
- Morley, S. K., & Freeman, M. P. (2007). On the association between northward turnings of the interplanetary magnetic field and substorm onsets. *Geophysical Research Letters*, *34*, L08104. <https://doi.org/10.1029/2006GL028891>
- Morley, S. K., Friedel, R. H. W., Spanswick, E. L., Reeves, G. D., Steinberg, J. T., Koller, J., et al. (2010). Dropouts of the outer electron radiation belt in response to solar wind stream interfaces: Global positioning system observations. *Proceedings of The Royal Society A*, *466*, 3329–3350.
- Newell, P. T., Liou, K., Gjerloev, J. W., Sotirelis, T., Wing, S., & Mitchell, E. J. (2016). Substorm probabilities are best predicted from solar wind speed. *Journal of Atmospheric and Solar-Terrestrial Physics*, *146*, 28–37.
- Ni, B., Bortnik, J., Thorne, R. M., Ma, Q., & Chen, L. (2013). Resonant scattering and resultant pitch angle evolution of relativistic electrons by plasmaspheric hiss. *Journal of Geophysical Research: Space Physics*, *118*, 7740–7751. <https://doi.org/10.1002/2013JA019260>
- Nosé, M., Iyemori, T., Sugiura, M., & Slavin, J. A. (1995). A strong dawn/dusk asymmetry in Pc5 pulsation occurrence observed by the DE-1 satellite. *Geophysical Research Letters*, *22*, 2053–2056.
- O'Brien, T. P., Lorentzen, K. R., Mann, I. R., Meredith, N. P., Blake, J. B., Fennell, J. F., et al. (2003). Energization of relativistic electrons in the presence of ULF power and MeV microbursts: Evidence for dual ULF and VLF acceleration. *Journal of Geophysical Research*, *108*(A8), 1329. <https://doi.org/10.1029/2002JA009784>
- O'Brien, T. P., McPherron, R. L., Sornette, D., Reeves, G. D., Friedel, R., & Singer, H. J. (2001). Which magnetic storms produce relativistic electrons at geosynchronous orbit? *Journal of Geophysical Research*, *106*(A8), 15,533–15,544.
- O'Brien, T. P., & Moldwind, M. B. (2003). Empirical plasmopause models from magnetic indices. *Geophysical Research Letters*, *30*(4), 1152. <https://doi.org/10.1029/2002GL016007>
- O'Brien, T. P., Sornette, D., & McPherron, R. L. (2001). Statistical asynchronous regression: Determining the relationship between two quantities that are not measured simultaneously. *Journal of Geophysical Research*, *106*, 13,247–13,259.
- Onsager, T. G., Green, J. C., Reeves, G. D., & Singer, H. J. (2012). Solar wind and magnetospheric conditions leading to the abrupt loss of outer radiation belt electrons. *Journal of Geophysical Research*, *117*, A01202. <https://doi.org/10.1029/2006JA011708>
- Onsager, T., Grubb, R., Kunches, J., Matheson, L., Speich, D., Zwickl, R. W., & Sauer, H. (1996). Operational uses of GOES energetic particle detectors. In E. R. Washwell (Ed.), *GOES-8 and beyond*, SPIE Proc. Ser. 2812 (Vol. 281, pp. 281–290). Boulder, CO.
- Ozeke, L. G., Mann, I. R., Murphy, K. R., Rae, I. J., Milling, D. K., Elkington, S. R., et al. (2012). ULF wave derived radiation belt radial diffusion coefficients. *Journal of Geophysical Research*, *117*, A04222. <https://doi.org/10.1029/2011JA017463>
- Ozeke, L. G., Mann, I. R., Turner, D. L., Murphy, K. R., Degeling, A. W., Rae, I. J., & Milling, D. K. (2014). Modeling cross L-shell impacts of magnetopause shadowing and ULF wave radial diffusion in the Van Allen belts. *Geophysical Research Letters*, *41*, 6556–6562. <https://doi.org/10.1002/2014GL060787>

- Paulikas, G. A., & Blake, J. B. (1979). Effects of the solar wind on magnetospheric dynamics: Energetic electrons at geosynchronous orbit, in Quantitative Modeling of Magnetospheric Processes. *Geophysical Monograph Series*, 21, 180–202.
- Posch, J. L., Engebretson, M. J., Pilipenko, V. A., Hughes, W. J., Russell, C. T., & Lanzerotti, L. J. (2003). Characterizing the long-period ULF response to magnetic storms. *Journal of Geophysical Research*, 108(A1), 1029. <https://doi.org/10.1029/2002JA009386>
- Rae, I. J., Mann, I. R., Murphy, K. R., Ozeke, L. G., Milling, D. K., Chan, A. A., et al. (2012). Ground-based magnetometer determination of in situ Pc4-5 ULF electric field wave spectra as a function of solar wind speed. *Journal of Geophysical Research*, 117, A04221. <https://doi.org/10.1029/2011JA017335>
- Rae, I. J., Mann, I. R., Watt, C. E., Kistler, L. M., & Baumjohann, W. (2007). Equator-s observations of drift mirror mode waves in the dawnside magnetosphere. *Journal of Geophysical Research*, 112, A11203. <https://doi.org/1029/2006JA0012604>
- Reeves, G. D., McAdams, K. L., Friedel, R. H. W., & O'Brien, T. P. (2003). Acceleration and loss of relativistic electrons during geomagnetic storms. *Geophysical Research Letters*, 30(10), 1529. <https://doi.org/10.1029/2002GL016513>
- Reeves, G., Morley, S., & Cunningham, G. (2013). Long-term variations in solar wind velocity and radiation belt electrons. *Journal of Geophysical Research: Space Physics*, 118, 1040–1048. <https://doi.org/10.1002/jgra.50126>
- Reeves, G. D., Morley, S. K., Friedel, R. H. W., Henderson, M. G., Cayton, T. E., Cunningham, G., et al. (2011). On the relationship between relativistic electron flux and solar wind velocity: Paulikas and Blake revisited. *Journal of Geophysical Research*, 116, A02213. <https://doi.org/10.1029/2010JA015735>
- Richardson, I. G., & Cane, H. V. (2004). The fraction of interplanetary coronal mass ejections that are magnetic clouds: Evidence for a solar cycle variation. *Geophysical Research Letters*, 31, L18804. <https://doi.org/10.1029/2004GL020958>
- Richardson, I. G., & Cane, H. V. (2010). Near-Earth interplanetary coronal mass ejections during solar cycle 23 (1996–2009): Catalog and summary of properties. *Solar Physics*, 264, 189–237.
- Rodger, C. J., Cresswell-Moorcock, K., & Clilverd, M. A. (2016). Nature's grand experiment: Linkage between magnetospheric convection and the radiation belts. *Journal of Geophysical Research: Space Physics*, 121, 171–189. <https://doi.org/10.1002/2015JA021537>
- Roederer, J. G. (1970). Periodic drift motion and conservation of the third adiabatic invariant. In *Dynamics of geomagnetically trapped radiation* (pp. 72–82). Berlin-Heidelberg: Springer.
- Samson, J. C., & Rostoker, G. (1972). Latitude-dependent characteristics of high-latitude Pc4 and Pc5 micropulsations. *Journal of Geophysical Research*, 77, 6133–6144.
- Sarris, T. E., Loto'aniu, T. M., Li, X., & Singer, H. J. (2007). Observations at geosynchronous orbit of a persistent Pc5 geomagnetic pulsation and energetic electron flux modulations. *Annales Geophysicae*, 25, 1653–1667.
- Shprits, Y. Y., Thorne, R. M., Friedel, R., Reeves, G. D., Fennell, J., Baker, D. N., & Kanekal, S. G. (2006). Outward radial diffusion driven by losses at the magnetopause. *Journal of Geophysical Research*, 111, A11214. <https://doi.org/10.1029/2006JA011657>
- Shue, J.-H., Song, P., Russell, C. T., Steinberg, J. T., Chao, J. K., Zastenker, G., et al. (2006). Magnetopause location under extreme solar wind conditions. *Journal of Geophysical Research*, 103, 17,691–17,700. <https://doi.org/10.1029/98JA01103>
- Simms, L. E., Pilipenko, V., Engebretson, M. J., Reeves, G. D., Smith, A. J., & Clilverd, M. (2014). Prediction of relativistic electron flux at geostationary orbit following storms: Multiple regression analysis. *Journal of Geophysical Research: Space Physics*, 119, 7297–7318. <https://doi.org/10.1002/2014JA019955>
- Song, X.-T., Gendrin, R., & Caudal, G. (1988). Refilling process in the plasmasphere and its relation to magnetic activity. *Journal of Atmospheric and Solar-Terrestrial Physics*, 50(3), 185–195.
- Su, Z., Zhu, H., Xiao, F., Zong, Q.-G., Zhou, X.-Z., Zheng, H., et al. (2015). Ultra-low-frequency wave-driven diffusion of radiation belt relativistic electrons. *Nature Communications*, 6, 10096.
- Subbotin, D. A., & Shprits, Y. Y. (2009). Three-dimensional modeling of the radiation belts using the Versatile Electron Radiation Belt (VERB) code. *Space Weather*, 7, S10001. <https://doi.org/10.1029/2008SW000452>
- Summers, D., Thorne, R. M., & Xiao, F. (1998). Relativistic theory of wave-particle resonant diffusion with application to electron acceleration in the magnetosphere. *Journal of Geophysical Research*, 103, 20,487–20,500.
- Tu, W., Selesnick, R., Li, X., & Looper, M. (2010). Quantification of the precipitation loss of radiation belt electrons observed by SAMPEX. *Journal of Geophysical Research*, 115, A07210. <https://doi.org/10.1029/2009JA014949>
- Turner, D. L. (2010). Earth's outer radiation belt electrons: Identifying sources, improving forecasts, and a new particle detector design (PhD thesis).
- Tverskaya, L. V., Ivanova, T. A., Pavlov, N. N., Reizman, S. Y., Rubinstein, I. A., Sosnovets, E. N., & Vedek'kin, N. N. (2003). Predicting the L-position of the storm-injected relativistic electron belt. *Advances in Space Research*, 31(4), 1039–1044.
- Ukhorskiy, A. Y., Sitnov, M. I., Millan, R. M., Kress, B. T., Fennell, J. F., Claudepierre, S. G., & Barnes, R. J. (2015). Global storm time depletion of the outer electron belt. *Journal of Geophysical Research: Space Physics*, 120, 2543–2556. <https://doi.org/10.1002/2014JA020645>
- Van Allen, J. A., Ludwig, G. H., Ray, E. C., & McIlwain, C. E. (1958). Observation of high intensity radiation by satellites 1958 Alpha and Gamma. *Jet Propulsion*, 28, 588–592.
- Williams, D. J., Arens, L. J., & Lanzerotti, L. I. (1968). Observations of trapped electrons at low and high altitudes. *Journal of Geophysical Research*, 73, 5673–5696.
- Wing, S., Johnson, J. R., Camporeale, E., & Reeves, G. D. (2017). Information theoretical approach to discovering solar wind drivers of the outer radiation belt. *Journal of Geophysical Research: Space Physics*, 121, 9378–9399. <https://doi.org/10.1002/2016JA022711>
- Yokoyama, N., & Kamide, Y. (1997). Statistical nature of geomagnetic storms. *Journal of Geophysical Research*, 102(A7), 14,215–14,222.
- Yu, Y., Koller, J., & Morley, S. K. (2013). Quantifying the effect of magnetopause shadowing on electron radiation belt dropouts. *Annales Geophysicae*, 31, 1929–1939.
- Zhang, J., Richardson, I. G., Webb, D. F., Gopalswamy, N., Huttunen, E., Kasper, J. C., et al. (2007). Solar and interplanetary sources of major geomagnetic storms (Dst < -100 nT) during 1996–2005. *Journal of Geophysical Research*, 112, A12103. <https://doi.org/10.1029/2007JA012321>
- Zhao, H., Baker, D. N., Jaynes, A. N., Li, X., Elkington, S. R., Kanekal, S. G., et al. (2017). On the relation between radiation belt electrons and solar wind parameters/geomagnetic indices: Dependence of the first adiabatic invariant and L\*. *Journal of Geophysical Research: Space Physics*, 122, 1624–1642. <https://doi.org/10.1002/2016JA023658>
- Zhao, H., & Li, X. (2013). Inward shift of the outer radiation belt electrons as a function of Dst index and the influence of the solar wind on electron injections into the slot region. *Journal of Geophysical Research: Space Physics*, 118, 756–764. <https://doi.org/10.1029/2012JA018179>